



**Continuous Kubo-Greenwood formula: Theory and numerical implementation**G. S. Demyanov <sup>\*</sup>, D. V. Knyazev , and P. R. Levashov *Joint Institute for High Temperatures, Izhor'skaya 13 Building 2, Moscow 125412, Russia  
and Moscow Institute of Physics and Technology, Institut'skiy Pereulok 9, Dolgoprudny, Moscow Region 141700, Russia*

(Received 28 October 2021; accepted 2 March 2022; published 28 March 2022)

In this paper, we present the so-called continuous Kubo-Greenwood formula intended for the numerical calculation of the dynamic Onsager coefficients and, in particular, the real part of dynamic electrical conductivity. In contrast to the usual Kubo-Greenwood formula, which contains the summation over a discrete set of transitions between electron energy levels, the continuous one is formulated as an integral over the whole energy range. This integral includes the continuous functions: the smoothed squares of matrix elements,  $D(\varepsilon, \varepsilon + \hbar\omega)$ , the densities of state,  $g(\varepsilon)g(\varepsilon + \hbar\omega)$ , and the difference of the Fermi weights,  $[f(\varepsilon) - f(\varepsilon + \hbar\omega)]/(\hbar\omega)$ . The function  $D(\varepsilon, \varepsilon + \hbar\omega)$  is obtained via the specially developed smoothing procedure. From the theoretical point of view, the continuous formula is an alternative to the usual one. Both can be used to calculate matter properties and produce close results. However, the continuous formula includes the smooth functions that can be plotted and examined. Thus, we can analyze the contributions of various parts of the electron spectrum to the obtained properties. The possibility of such analysis is the main advantage of the continuous formula. The continuous Kubo-Greenwood formula is implemented in the parallel code CUBOGRAM. Using the code we demonstrate the influence of technical parameters on the simulation results for liquid aluminum. We also analyze various methods of matrix elements computation and their effect on dynamic electrical conductivity.

DOI: [10.1103/PhysRevE.105.035307](https://doi.org/10.1103/PhysRevE.105.035307)**I. INTRODUCTION**

Electronic transport and optical properties in condensed media are useful in many applications including astrophysics [1,2], laser-matter interaction [3], electrophysics [4], shock-wave physics [5], and plasma physics [6]. In our paper, we refer to frequency-dependent electrical conductivity, static electrical and thermal conductivity as transport and optical properties. Wide-range models of these properties are important for continuum mechanics simulation of laser experiments with condensed targets [3,7]. However, strong interparticle interaction and degeneracy effects significantly hamper the theoretical consideration of transport and optical phenomena in dense media. Hence, such wide-range models are still rather rare [8,9].

A number of approaches have been worked out to calculate transport and optical properties in plasma. Kinetic methods are based upon the solution of a classical or quantum kinetic equation. As the collision integral is unknown in most cases, the so-called  $\tau$  approximation is often used (see the well-known model by Lee and More [10]). Plasma composition can be also taken into account, for example, on the basis of the chemical picture [11–15] or electron jellium [16–18] models. At higher density it is possible to consider a coherent scattering of quantum electrons on ions with the spatial arrangement defined by a structure factor. This semiphenomenological theory proposed by Ziman [19] shows satisfactory results for liquid metals at relatively low temperatures [20]. Nevertheless, contradictory results are obtained in dense plasma in the

case of significant interaction and quantum effects. It occurs due to uncertainties with collision integrals and the form of a kinetic equation itself.

Hence, a linear response theory (LRT) is usually used in condensed media, although alternative more general methods based upon an effective static approximation [21] and time-dependent density functional theory (DFT) [22,23] are actively being developed. In the LRT it is possible, in principle, to take into account complex many-particle interaction both in classical and quantum cases. This leads to the famous Green-Kubo [24,25] and Kubo-Greenwood (KG) [26] formulas that currently are widely used in classical and quantum statistical physics. In particular, impressive results were obtained for transport and optical properties of liquid metals and dense metallic plasma using DFT and quantum molecular dynamics (QMD) [27–31].

However, many of the papers employing the QMD+KG technique have the following features. The calculation is performed via the common numerical implementation of the Kubo-Greenwood formula, that we call the usual formula [Eq. (5)]. In this type of computation, the transitions of electrons between various initial and final states are taken into account, and the final values of transport and optical properties are formed. The calculation is performed using off-the-shelf software, and its details are not obvious to an ordinary user. Often the only quantities to be understood and discussed are the final values of transport and optical properties [27–29,32–34].

In this paper, we propose another numerical implementation of the Kubo-Greenwood formula. We compute the following smooth functions using the results of QMD+DFT calculation: smoothed squares of matrix elements (SSME)

<sup>\*</sup>Corresponding author: demyanov.gs@phystech.edu

$D(\varepsilon_1, \varepsilon_2)$ , density of states (DOS)  $g(\varepsilon)$ , and the Fermi-Dirac distribution  $f(\varepsilon)$ . Then the integral of expression  $D(\varepsilon, \varepsilon)g^2(\varepsilon)(-\frac{\partial f}{\partial \varepsilon}(\varepsilon))$  yields the static electrical conductivity  $\sigma_{1DC}$ . We call the corresponding Eq. (23) the *continuous Kubo-Greenwood formula* for the static electrical conductivity. Similar expressions are available for dynamic electrical conductivity [Eq. (22)] and thermal conductivity [Eq. (26)].

The continuous Kubo-Greenwood formula yields transport and optical properties as the usual one. Later we will show that both expressions produce rather close results (Sec. IV C). However, the continuous formula makes it possible to analyze how transport and optical properties are formed. In contrast to the usual formula, the continuous one includes the smooth functions  $D(\varepsilon, \varepsilon)$ ,  $g^2(\varepsilon)$ , and  $-\frac{\partial f}{\partial \varepsilon}(\varepsilon)$ . These functions can be plotted and examined. Thus we can find out the parts of the spectrum which contribute mostly to transport and optical properties. In our paper, we demonstrate an example of such analysis for liquid aluminum (Sec. V). The influence of density and temperature on final results can be understood better by studying their effect on the functions  $D(\varepsilon, \varepsilon)$ ,  $g^2(\varepsilon)$ , and  $-\frac{\partial f}{\partial \varepsilon}(\varepsilon)$ . The possibility of such detailed analysis is an advantage of the continuous formula.

The article is organized as follows. Section II contains the description of computational technique based on QMD and the usual Kubo-Greenwood formula. In Sec. III we provide the derivation of the continuous Kubo-Greenwood formula, including our smoothing procedure. Section IV deals with the discussion of advantages of the continuous Kubo-Greenwood formula and its equivalence to the usual formula in the limit of zero  $\delta$ -function broadening. An example of a calculation using the continuous Kubo-Greenwood formula is given in Sec. V. In Sec. VI we particularly discuss technical parameters of QMD simulation, the dependence of results on the  $\delta$ -function broadening, and the method of matrix elements calculation. After the presentation of all our results, we perform a detailed consideration of related ideas in previous works (Sec. VII). Thus we estimate the position of our work among others. We summarize our study in Sec. VIII.

## II. CALCULATION OF TRANSPORT AND OPTICAL PROPERTIES USING THE USUAL KUBO-GREENWOOD FORMULA

In this work, we calculate transport and optical properties using the usual and the continuous Kubo-Greenwood formulas. The latter will be introduced in Sec. III. In our earlier paper [35], the usual Kubo-Greenwood formula was used. The most basic points about the technique of calculating the transport and optical properties via the usual formula will be discussed here. For a more detailed consideration, one could refer to [35].

In this section, we explain the meaning of various technical parameters; their specific numerical values will be available in Sec. VIA. For the usual Kubo-Greenwood formula, we have discussed many questions concerning the influence of technical parameters and convergence in our previous paper (see Sec. 3 of [35]). Additional information on convergence is also presented in Sec. VIA.

The computation method consists of three main stages: QMD simulation, the precise calculation of the band structure,

and the calculation of the transport and optical properties using the Kubo-Greenwood formula. The first two stages are carried out using the Vienna *Ab Initio* Simulation Package (VASP) [36–38]. The final stage is performed via a parallel **Greenwood-Kubo** Program (GREEKUP) [39], written by the authors of this paper.

At the first stage  $N_{at}$  atoms are placed to face-centered cubic (fcc) positions in a cubic supercell with periodic boundary conditions. The supercell volume  $\Omega$  is chosen to achieve the certain density  $\rho$  for a given number of atoms.

For these initial positions of ions, the electronic structure is calculated within the framework of DFT by solving the finite-temperature Kohn-Sham equations. The electron temperature  $T_e$  is a parameter of the Fermi-Dirac distribution  $f(\varepsilon)$ . The electrons are completely adjusted to the positions of ions, which is the Born-Oppenheimer approximation.

Since the electronic structure is calculated, forces acting on ions from electrons and other ions could be obtained from the Hellmann-Feynman theorem. The positions of ions are also influenced by the presence of the Nosé thermostat, which maintains the ionic subsystem at an ion temperature  $T_i$ . These forces are used to calculate the positions of ions at the next step of QMD simulation in the *NVT* ensemble.

In this work, we consider the case of equal electron and ion temperatures ( $T_e = T_i$ ). However, the two-temperature case ( $T_e \neq T_i$ ) is also possible for analysis [40].

As a result of the first stage of the calculation, we obtain trajectories of ions, as well as the time dependencies of the total energy  $E(t)$  and the pressure  $p(t)$  of the system for a discrete set of moments  $t_s$ . By averaging these time dependencies over the equilibrium section, one could find the thermodynamic energy  $E$  and pressure  $p$  of the system.

At the second stage of the calculation, several independent ionic configurations are selected from the equilibrium section of the QMD simulation performed at the first stage. A detailed calculation of the band structure is performed for each selected configuration. The calculation of the electronic structure is carried out similarly to the first stage, but a larger number of  $\mathbf{k}$  points, a larger number of electron bands,  $N_{bands}$ , and, if necessary, a larger cutoff energy  $E_{cut}$  are used. As a result, we get the Kohn-Sham energy eigenvalues  $\varepsilon_{i,\mathbf{k}}$  for different  $\mathbf{k}$  points in the Brillouin zone, the corresponding wave functions  $|\Psi_{i,\mathbf{k}}\rangle$ , and the Fermi weights  $f(\varepsilon_{i,\mathbf{k}})$ . Various  $\mathbf{k}$  points are taken into account with the weights  $W(\mathbf{k})$ . The chemical potential  $\mu$  and dipole matrix elements (in terms of momentum) are also obtained. Here  $i$  is the number of the electronic band. The energy eigenvalues  $\varepsilon_{i,\mathbf{k}}$  form the discrete spectrum.

At the third stage the accumulated information is used to calculate transport and optical properties.

Consider now the effect of an electric field pulse  $\mathbf{E}(t)$  on the electronic subsystem. A conduction current with the electric current density  $\mathbf{j}(t)$  arises due to this pulse. The Fourier transform produces the components of the electric field  $\mathbf{E}(\omega)$  and the electric current density  $\mathbf{j}(\omega)$  corresponding to a frequency  $\omega$ . These Fourier components are connected through the dynamic electrical conductivity  $\sigma(\omega) = \sigma_1(\omega) + i\sigma_2(\omega)$  (in an isotropic medium):

$$\mathbf{j}(\omega) = (\sigma_1(\omega) + i\sigma_2(\omega))\mathbf{E}(\omega). \quad (1)$$

The real part of the dynamic electrical conductivity is given by the *exact Kubo-Greenwood formula* [41]:

$$\sigma_1(\omega) = \frac{2\pi e^2 \hbar^3}{m_e^2 \Omega} \sum_{\substack{i,j,\mathbf{k} \\ i \neq j}} W(\mathbf{k}) D_{ij}^{\mathbf{k}} \times \frac{f(\varepsilon_{i,\mathbf{k}}) - f(\varepsilon_{j,\mathbf{k}})}{\hbar\omega} \delta(\varepsilon_{j,\mathbf{k}} - \varepsilon_{i,\mathbf{k}} - \hbar\omega). \quad (2)$$

Here,  $e$  is the electron charge ( $e > 0$ ),  $m_e$  denotes the electron mass, and  $\hbar$  is the Planck constant. Also,  $D_{ij}^{\mathbf{k}}$  denotes the dipole matrix element squared in terms of the momentum operator, averaged over spatial directions. In the case of a local effective potential in the Kohn-Sham equations, this matrix element reduces to a matrix element of the gradient operator  $\langle \Psi_{i,\mathbf{k}} | \nabla_\alpha | \Psi_{j,\mathbf{k}} \rangle$ :

$$D_{ij}^{\mathbf{k}} = \frac{1}{3} \sum_{\alpha} |\langle \Psi_{i,\mathbf{k}} | \nabla_\alpha | \Psi_{j,\mathbf{k}} \rangle|^2, \quad (3)$$

where  $\alpha$  denotes three spatial directions. The case of a nonlocal potential will be discussed later in Sec. VID 1 d. Moreover,  $D_{ij}^{\mathbf{k}}$  can be calculated via several numerical methods; this will be discussed in Sec. VID.

The Kubo-Greenwood formula is originally derived from the general principles of LRT, but its implementation with the Kohn-Sham wave functions and energy eigenvalues is an approximation. Nevertheless, we use the term “exact” for Eq. (2) as the designation for the Kubo-Greenwood formula with an exact  $\delta$  function, although with the Kohn-Sham wave functions.

The exact  $\delta$  function is replaced by the broadened  $\delta$  function with a broadening  $\Delta E$ ,

$$\delta(\varepsilon_{j,\mathbf{k}} - \varepsilon_{i,\mathbf{k}} - \hbar\omega) \rightarrow \delta_{\Delta E}(\varepsilon_{j,\mathbf{k}} - \varepsilon_{i,\mathbf{k}} - \hbar\omega), \quad (4)$$

in the common numerical implementation of Eq. (2):

$$\sigma_1^{KG}(\omega) = \frac{2\pi e^2 \hbar^3}{m_e^2 \Omega} \sum_{\substack{i,j,\mathbf{k} \\ i \neq j}} W(\mathbf{k}) D_{ij}^{\mathbf{k}} \times \frac{f(\varepsilon_{i,\mathbf{k}}) - f(\varepsilon_{j,\mathbf{k}})}{\hbar\omega} \delta_{\Delta E}(\varepsilon_{j,\mathbf{k}} - \varepsilon_{i,\mathbf{k}} - \hbar\omega). \quad (5)$$

In this work, we call Eq. (5) the *usual Kubo-Greenwood formula*. Equation (5) is equivalent to the exact formula (2) in the limit  $\Delta E \rightarrow 0$ . A calculation via the usual Kubo-Greenwood formula is marked by the index “KG”. This type of calculation involves the summation over a discrete set of transitions and the usage of a broadened  $\delta$  function. The usual Kubo-Greenwood formula (5) is used to obtain dynamic electrical conductivity at the third stage of calculation.

In this work, the Gaussian [27] broadening (40) is used during the calculation via the usual KG formula (5). The choice of the broadening parameter  $\Delta E$  is an important issue. One should study the dependence of the calculated  $\sigma_1^{KG}(\omega)$  curves on  $\Delta E$  to obtain correct results. The procedure for determining the optimal value of  $\Delta E$  was investigated in our previous work [35].

The dynamic Onsager coefficients  $L_{mn}^{KG}(\omega)$  are also calculated using the usual Kubo-Greenwood formula [32,35,39]:

$$L_{mn}^{KG}(\omega) = (-1)^{m+n} \frac{1}{e^{m-1} (eT_e)^{n-1}} \frac{2\pi e^2 \hbar^3}{m_e^2 \Omega} \times \sum_{\substack{i,j,\mathbf{k} \\ i \neq j}} W(\mathbf{k}) \left( \frac{\varepsilon_{i,\mathbf{k}} + \varepsilon_{j,\mathbf{k}}}{2} - \mu \right)^{m+n-2} \times D_{ij}^{\mathbf{k}} \frac{f(\varepsilon_{i,\mathbf{k}}) - f(\varepsilon_{j,\mathbf{k}})}{\hbar\omega} \delta_{\Delta E}(\varepsilon_{j,\mathbf{k}} - \varepsilon_{i,\mathbf{k}} - \hbar\omega). \quad (6)$$

The static Onsager coefficients are obtained by extrapolating  $L_{mn}^{KG}(\omega)$  to zero frequency:  $L_{mn}^{KG} = \lim_{\omega \rightarrow 0} L_{mn}^{KG}(\omega)$ .

Note that  $\sigma_1^{KG}(\omega) \equiv L_{11}^{KG}(\omega)$  and  $\sigma_{1DC}^{KG} \equiv L_{11}^{KG}$ . Knowing  $L_{mn}^{KG}$ , one could also obtain the thermal conductivity  $K^{KG}$ :

$$K^{KG} = L_{22}^{KG} - \frac{L_{12}^{KG} L_{21}^{KG}}{L_{11}^{KG}}. \quad (7)$$

Thus, thermal conductivity differs from  $L_{22}^{KG}$  by the thermoelectric term. But for the temperature  $k_B T_e \ll E_F$  considered in this paper, the approximation  $K^{KG} \approx L_{22}^{KG}$  can be used. Here,  $k_B$  is the Boltzmann constant and  $E_F$  is the Fermi energy.

At the third stage of calculation the GREEKUP code is used to obtain electrical and thermal conductivities via the usual Kubo-Greenwood formula (6).

In this paper we calculate the electronic DOS as the sum of the broadened  $\delta$  functions:

$$g_{\mathbf{k}}(\varepsilon) = \sum_i \delta_{\Delta E_{DOS}}(\varepsilon - \varepsilon_{i,\mathbf{k}}). \quad (8)$$

This calculation is performed for each chosen ionic configuration and each  $\mathbf{k}$  point. Note that the broadening  $\Delta E_{DOS}$  could differ from  $\Delta E$ . The total density of electronic states,  $g(\varepsilon)$ , is obtained by averaging  $g_{\mathbf{k}}(\varepsilon)$  over the  $\mathbf{k}$  points and ionic configurations:

$$g(\varepsilon) = \left\langle \sum_{\mathbf{k}} W(\mathbf{k}) g_{\mathbf{k}}(\varepsilon) \right\rangle. \quad (9)$$

Here,  $\langle \dots \rangle$  means the average over ionic configurations.

Thus, it is possible to calculate the optical and transport properties and DOS of the considered system. The structure of the matrix elements squared,  $D_{ij}^{\mathbf{k}}$ , should be known for this calculation, since they determine the values of electrical and thermal conductivities.

We come now to the problem of calculating a specific continuous and smooth function  $D(\varepsilon_1, \varepsilon_2)$ , which would show the dependence of the dipole matrix elements on the energies of the initial and final states:  $D(\varepsilon_1, \varepsilon_2) \propto D_{ij}$ .

We now suggest the procedure for calculating such a function. It will be calculated directly from the matrix elements squared,  $D_{ij}^{\mathbf{k}}$ , and energy levels  $\varepsilon_{i,\mathbf{k}}$ . A relationship between this function and all the Onsager coefficients will be also demonstrated.

### III. CONTINUOUS KUBO-GREENWOOD FORMULA

The calculation of optical and transport properties could be carried out according to the usual Kubo-Greenwood

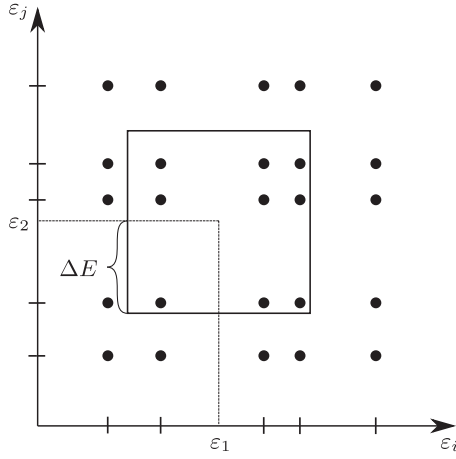


FIG. 1. Illustration of the averaging algorithm. The energy of the initial state participating in transition is plotted along the horizontal axis, whereas the energy of the final state is plotted along the vertical axis. The black dots represent transitions. Every transition possesses its matrix element squared  $D_{ij}$ . The square  $\Pi$  of a size  $2\Delta E \times 2\Delta E$  centered at the point  $(\varepsilon_1, \varepsilon_2)$  is also shown. Matrix elements inside the square  $\Pi$  are taken into account to calculate the average of  $D_{ij}$ . This average is referred to the point  $(\varepsilon_1, \varepsilon_2)$ .

formula (5). It includes  $\frac{f(\varepsilon_i) - f(\varepsilon_j)}{\hbar\omega}$ , the broadened  $\delta$  function  $\delta_{\Delta E}(\varepsilon_j - \varepsilon_i - \hbar\omega)$ , and matrix elements squared  $D_{ij}$ .

However, it is almost impossible to study  $D_{ij}$  directly. They represent a discrete set of values for various transitions (Fig. 2, left). Because of this, it remains hidden how the electrical conductivity  $\sigma_1^{KG}(\omega)$  and thermal conductivity  $K^{KG}$  are formed. We will develop a specific approach to study matrix elements squared  $D_{ij}$  as a continuous function.

For simplicity, the entire theoretical consideration in this section is performed only for one  $\mathbf{k}$  point.

### A. Averaging and smoothing of the matrix elements squared

Matrix elements squared  $D_{ij}$  are present in the exact Kubo-Greenwood formula (2). They show the intensity of

a transition between one-electron levels. We now introduce an averaging and smoothing procedure to analyze the energy dependence of  $D_{ij}$ .

The summation in the exact Kubo-Greenwood formula (2) runs over all  $i \neq j$ . Equation (2) can be rewritten in an equivalent way with the summation over *all*  $i$  and  $j$ , if we formally set diagonal  $D_{ii}$  to zero. The latter formulation is convenient during the further consideration. We assume  $D_{ii} = 0$  in the following averaging and smoothing procedure.

We introduce an auxiliary function  $h(\varepsilon_1, \varepsilon_2)$ :

$$h(\varepsilon_1, \varepsilon_2)|_{(\varepsilon_1, \varepsilon_2) = (\varepsilon_i, \varepsilon_j)} \equiv D_{ij}, \quad (10)$$

where  $\varepsilon_i, \varepsilon_j$  are some eigenvalues of the considered system. The function  $h(\varepsilon_1, \varepsilon_2)$  is equal to 0 in other cases.

Let us use the rectangular function with a half width  $\Delta E$  to broaden the  $\delta$ -function:

$$\delta_{\Delta E}(\varepsilon - \varepsilon_i) = \begin{cases} \frac{1}{2\Delta E}, & \text{if } \varepsilon_i - \Delta E \leq \varepsilon \leq \varepsilon_i + \Delta E \\ 0, & \text{otherwise.} \end{cases} \quad (11)$$

The density of states  $g(\varepsilon)$  is given by

$$g(\varepsilon) = \sum_i \delta_{\Delta E}(\varepsilon - \varepsilon_i). \quad (12)$$

Consider now a square  $\Pi$  of the size  $2\Delta E \times 2\Delta E$  centered at some point  $(\varepsilon_1, \varepsilon_2)$  (Fig. 1). Let us find the sum of  $D_{ij}$  contained in  $\Pi$ ,

$$\begin{aligned} \sum_{(\varepsilon_i, \varepsilon_j) \in \Pi} h(\varepsilon_i, \varepsilon_j) &= \sum_{i,j} h(\varepsilon_i, \varepsilon_j) \\ &\times \delta_{\Delta E}(\varepsilon_1 - \varepsilon_i) \delta_{\Delta E}(\varepsilon_2 - \varepsilon_j) (2\Delta E)^2, \end{aligned} \quad (13)$$

and their number as well:

$$\sum_{(\varepsilon_i, \varepsilon_j) \in \Pi} 1 = \sum_{i,j} \delta_{\Delta E}(\varepsilon_1 - \varepsilon_i) \delta_{\Delta E}(\varepsilon_2 - \varepsilon_j) (2\Delta E)^2. \quad (14)$$

Here the broadened  $\delta$  functions work as indicator functions checking whether the matrix element is located inside the square  $\Pi$ . The average of these matrix elements

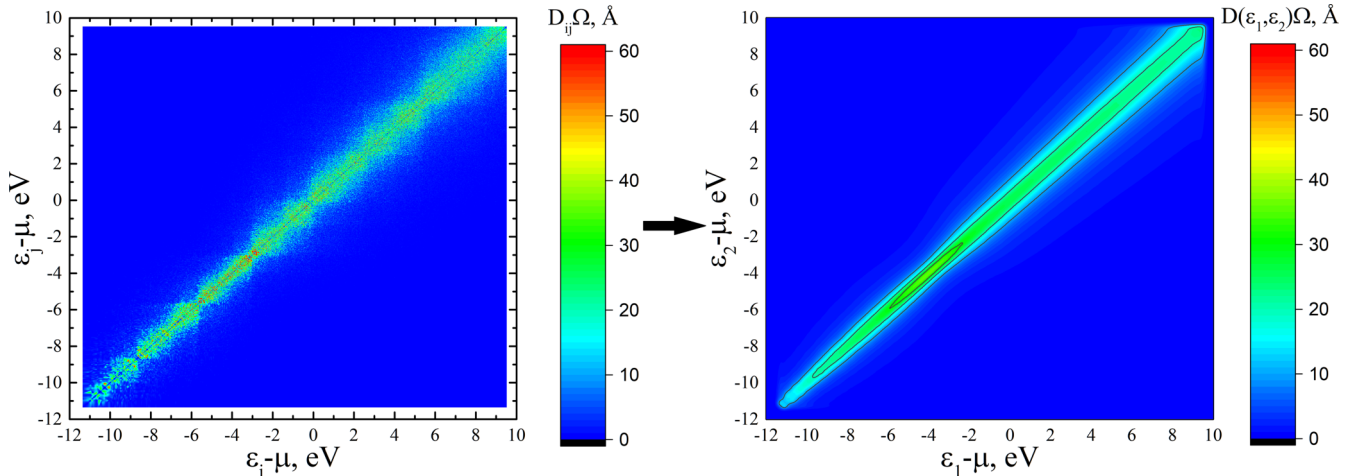


FIG. 2. Illustration of the procedure for averaging and smoothing  $D_{ij}$  [Eq. (16)]. Left: The matrix elements squared  $D_{ij}$  as a function of initial  $\varepsilon_i$  and final  $\varepsilon_j$  energies. Right: Smoothed squares of matrix elements  $D(\varepsilon_1, \varepsilon_2)$ . The discrete  $D_{ij}$  are plotted as a set of peaks, while  $D(\varepsilon_1, \varepsilon_2)$  is a smooth surface.

squared is

$$\frac{\sum_{i,j} h(\varepsilon_i, \varepsilon_j) \delta_{\Delta E}(\varepsilon_1 - \varepsilon_i) \delta_{\Delta E}(\varepsilon_2 - \varepsilon_j) (2\Delta E)^2}{\sum_{i,j} \delta_{\Delta E}(\varepsilon_1 - \varepsilon_i) \delta_{\Delta E}(\varepsilon_2 - \varepsilon_j) (2\Delta E)^2}. \quad (15)$$

This average value is now referred to the point  $(\varepsilon_1, \varepsilon_2)$ . Thus, using Eq. (10), we define the *smoothed squares of matrix elements* (SSME)  $D(\varepsilon_1, \varepsilon_2)$ :

$$D(\varepsilon_1, \varepsilon_2) = \frac{\sum_{i,j} D_{ij} \delta_{\Delta E}(\varepsilon_1 - \varepsilon_i) \delta_{\Delta E}(\varepsilon_2 - \varepsilon_j)}{\sum_i \delta_{\Delta E}(\varepsilon_1 - \varepsilon_i) \times \sum_j \delta_{\Delta E}(\varepsilon_2 - \varepsilon_j)}. \quad (16)$$

For convenience, we introduce the following function:

$$D_g(\varepsilon_1, \varepsilon_2) = \sum_{i,j} D_{ij} \delta_{\Delta E}(\varepsilon_1 - \varepsilon_i) \delta_{\Delta E}(\varepsilon_2 - \varepsilon_j). \quad (17)$$

The denominator of Eq. (16) could be rewritten in terms of DOS, whereas the numerator could be rewritten in terms of  $D_g(\varepsilon_1, \varepsilon_2)$ :

$$D(\varepsilon_1, \varepsilon_2) = \frac{D_g(\varepsilon_1, \varepsilon_2)}{g(\varepsilon_1)g(\varepsilon_2)}. \quad (18)$$

An illustration of the smoothing procedure is shown in Fig. 2.

The physical meaning of SSME is simple. The function  $D(\varepsilon_1, \varepsilon_2)$  shows the intensity of the electron transition between levels with energies  $\varepsilon_1$  and  $\varepsilon_2$ . The units of this function are the same as for the square of the matrix elements  $D_{ij}$ .

### B. Continuous formula for electrical conductivity and thermal conductivity

Let us find the relationship between SSME  $D(\varepsilon_1, \varepsilon_2)$  and the real part of the dynamic electrical conductivity using the exact Kubo-Greenwood formula.

The function  $D(\varepsilon_1, \varepsilon_2)$  shows the intensity of the electron transition between levels with energies  $\varepsilon_1, \varepsilon_2$ . The number of initial states in the energy range  $(\varepsilon_1 - d\varepsilon_1/2, \varepsilon_1 + d\varepsilon_1/2)$  is  $g(\varepsilon_1)d\varepsilon_1$ ; the number of final states in the energy range  $(\varepsilon_2 - d\varepsilon_2/2, \varepsilon_2 + d\varepsilon_2/2)$  is  $g(\varepsilon_2)d\varepsilon_2$ . Then, the sum of matrix elements squared for all transitions from the initial energy range to the final one is

$$D(\varepsilon_1, \varepsilon_2) \times g(\varepsilon_1)d\varepsilon_1 \times g(\varepsilon_2)d\varepsilon_2. \quad (19)$$

In the exact Kubo-Greenwood formula (2), the matrix element squared for each transition is multiplied by a factor  $\frac{f(\varepsilon_i) - f(\varepsilon_j)}{\hbar\omega} \delta(\varepsilon_j - \varepsilon_i - \hbar\omega)$ ; then, the contributions of these individual transitions are summed up. In terms of the continuous function  $D(\varepsilon_1, \varepsilon_2)$ , this could be expressed as

$$\iint D(\varepsilon_1, \varepsilon_2) g(\varepsilon_1) d\varepsilon_1 g(\varepsilon_2) d\varepsilon_2 \times \frac{f(\varepsilon_1) - f(\varepsilon_2)}{\hbar\omega} \delta(\varepsilon_2 - \varepsilon_1 - \hbar\omega). \quad (20)$$

Integration in Eq. (20) over the variable  $\varepsilon_2$  yields

$$\int d\varepsilon_1 D(\varepsilon_1, \varepsilon_1 + \hbar\omega) \times g(\varepsilon_1) g(\varepsilon_1 + \hbar\omega) \frac{f(\varepsilon_1) - f(\varepsilon_1 + \hbar\omega)}{\hbar\omega} \quad (21)$$

and, finally, the expression for the real part of the frequency-dependent conductivity:

$$\sigma_1^{CKG}(\omega) = \frac{2\pi e^2 \hbar^3}{m_e^2 \Omega} \int d\varepsilon D(\varepsilon, \varepsilon + \hbar\omega) \times g(\varepsilon) g(\varepsilon + \hbar\omega) \frac{f(\varepsilon) - f(\varepsilon + \hbar\omega)}{\hbar\omega}. \quad (22)$$

In this paper, Eq. (22) is called the *continuous Kubo-Greenwood formula*. Below (Sec. IV B) we will prove that the continuous formula (22) is equivalent to the exact one (2) in the limit  $\Delta E \rightarrow 0$ .

A calculation according to the continuous formula (22) is marked by the index ‘‘CKG’’. In this type of calculation, SSME  $D(\varepsilon_1, \varepsilon_2)$  and DOS  $g(\varepsilon_1), g(\varepsilon_2)$  are used.

Equation (22) has a clear physical meaning. The function  $D(\varepsilon, \varepsilon + \hbar\omega)$  presents the intensity of an electron transition from the energy level  $\varepsilon_1 = \varepsilon$  to  $\varepsilon_2 = \varepsilon + \hbar\omega$ . The relation  $\varepsilon_2 = \varepsilon_1 + \hbar\omega$  reflects the law of energy conservation. The full number of transitions is proportional to the DOS of initial and final states. The influence of the partial occupation of electronic levels is given by the function  $\frac{f(\varepsilon) - f(\varepsilon + \hbar\omega)}{\hbar\omega}$ . Integration over  $\varepsilon$  takes into account the transitions from all energy levels in the electron spectrum.

Passing to the limit  $\omega \rightarrow 0$ , one could obtain static electrical conductivity as an integral of the product of three continuous functions:

$$\sigma_{1DC}^{CKG} = \frac{2\pi e^2 \hbar^3}{m_e^2 \Omega} \int d\varepsilon D(\varepsilon, \varepsilon) g^2(\varepsilon) \left( -\frac{\partial f}{\partial \varepsilon}(\varepsilon) \right). \quad (23)$$

One could also obtain differential electrical conductivity  $\sigma_{1,\omega}(\varepsilon)$  at frequency  $\omega$ ,

$$\sigma_{1,\omega}^{CKG}(\varepsilon) = \frac{2\pi e^2 \hbar^3}{m_e^2 \Omega} D(\varepsilon, \varepsilon + \hbar\omega) \times g(\varepsilon) g(\varepsilon + \hbar\omega) \frac{f(\varepsilon) - f(\varepsilon + \hbar\omega)}{\hbar\omega}, \quad (24)$$

and in the limit  $\omega \rightarrow 0$ ,

$$\sigma_{1,0}^{CKG}(\varepsilon) = \frac{2\pi e^2 \hbar^3}{m_e^2 \Omega} D(\varepsilon, \varepsilon) g^2(\varepsilon) \left( -\frac{\partial f}{\partial \varepsilon}(\varepsilon) \right). \quad (25)$$

The integration of  $\sigma_{1,\omega}^{CKG}(\varepsilon)$  and  $\sigma_{1,0}^{CKG}(\varepsilon)$  over  $\varepsilon$  yields  $\sigma_1^{CKG}(\omega)$  and  $\sigma_{1DC}^{CKG}$ , respectively.

Following similar reasoning, one could find a connection between SSME and the Onsager coefficients:

$$L_{mn}^{CKG} = (-1)^{m+n} \frac{1}{e^{m-1} (eT_e)^{n-1}} \frac{2\pi e^2 \hbar^3}{m_e^2 \Omega} \times \int d\varepsilon (\varepsilon - \mu)^{m+n-2} D(\varepsilon, \varepsilon) g^2(\varepsilon) \left( -\frac{\partial f}{\partial \varepsilon}(\varepsilon) \right). \quad (26)$$

One could also obtain the differential Onsager coefficient  $L_{22,0}^{CKG}(\varepsilon)$ :

$$L_{22,0}^{CKG}(\varepsilon) = \frac{1}{e^2 T_e} \frac{2\pi e^2 \hbar^3}{m_e^2 \Omega} \times (\varepsilon - \mu)^2 D(\varepsilon, \varepsilon) g^2(\varepsilon) \left( -\frac{\partial f}{\partial \varepsilon}(\varepsilon) \right). \quad (27)$$

The presence of several  $\mathbf{k}$  points and ionic configurations is taken into account as follows:

$$D(\varepsilon_1, \varepsilon_2) = \frac{\langle \sum_{\mathbf{k}} W(\mathbf{k}) D_{\mathbf{k}}(\varepsilon_1, \varepsilon_2) g_{\mathbf{k}}(\varepsilon_1) g_{\mathbf{k}}(\varepsilon_2) \rangle}{\langle \sum_{\mathbf{k}} W(\mathbf{k}) g_{\mathbf{k}}(\varepsilon_1) \rangle \langle \sum_{\mathbf{k}} W(\mathbf{k}) g_{\mathbf{k}}(\varepsilon_2) \rangle}. \quad (28)$$

Functions  $g_{\mathbf{k}}(\varepsilon)$  and  $D_{\mathbf{k}}(\varepsilon_1, \varepsilon_2)$  are calculated by Eqs. (12) and (16), respectively, using energy levels and matrix elements squared corresponding to only one  $\mathbf{k}$  point.

### C. Numerical calculation according to the continuous formula using CUBOGRAM code

A numerical computation according to the continuous Kubo-Greenwood formula is started from the first two stages described in Sec. II: QMD simulation and precise calculation of the band structure.

However, the third stage of the calculation is different from that described in Sec. II. The third stage is performed using the parallel **Continuous Kubo–Greenwood Program** (CUBoGrAm) that we have created during the preparation of this paper.

The results obtained at the second stage via the VASP code are used as input information by CUBOGRAM. Primarily, CUBOGRAM requires dipole matrix elements in terms of the momentum operator (see Sec. VID) and energy levels  $\varepsilon_{i,\mathbf{k}}$ . While applying the continuous approach, functions  $f(\varepsilon)$  and  $-\frac{\partial f}{\partial \varepsilon}(\varepsilon)$  can be easily calculated directly for any  $\varepsilon$ . CUBOGRAM calculates DOS  $g(\varepsilon)$  and the function  $D_g(\varepsilon_1, \varepsilon_2)$  according to Eqs. (8) and (17), respectively, separately for each  $\mathbf{k}$  point. SSME are obtained via Eq. (18). Then, this information is used to calculate final DOS and SSME for several  $\mathbf{k}$  points and ionic configurations according to Eqs. (9) and (28), respectively.

CUBOGRAM calculates  $\sigma_1^{CKG}(\omega)$  according to the continuous Kubo-Greenwood formula (22). The Onsager coefficients  $L_{mn}^{CKG}$  are calculated using Eq. (26). These quantities are already averaged over  $\mathbf{k}$  points and ionic configurations since final DOS and SSME are used.

We consider that the calculation according to the continuous Kubo-Greenwood formula using CUBOGRAM is an alternative numerical implementation of the exact formula (2) (see Sec. IV B). The advantages of the continuous formula are discussed in Sec. IV A. The numerical results obtained via the usual and continuous Kubo-Greenwood formulas are compared in Sec. IV C.

## IV. USUAL AND CONTINUOUS KUBO-GREENWOOD FORMULAS

### A. Advantages of continuous formula

As already mentioned, the analysis of the usual Kubo-Greenwood formula (5) is challenging. As a result of the band structure calculation, matrix elements squared are obtained. Further, the final curve of dynamic electrical conductivity  $\sigma_1^{KG}(\omega)$  is calculated according to the usual Kubo-Greenwood formula. Within this approach, it is almost impossible to explain how the dependence  $\sigma_1^{KG}(\omega)$  is formed.

On the contrary, the continuous Kubo-Greenwood formula makes it possible to analyze the contributions to electrical and

thermal conductivity. The electrical conductivity is an integral of  $\sigma_{1,\omega}^{CKG}(\varepsilon)$ . The differential electrical conductivity includes the product of functions  $D(\varepsilon, \varepsilon + \hbar\omega)$ ,  $g(\varepsilon)g(\varepsilon + \hbar\omega)$ , and  $\frac{f(\varepsilon) - f(\varepsilon + \hbar\omega)}{\hbar\omega}$ .

These functions are smooth in our calculation; they can be graphed and examined. One can consider their dependence on the temperatures of ions and electrons, etc. One can also identify parts of the electronic spectrum that make the most substantial contribution to the conductivity value. Therefore, one could better understand the form of the final curve  $\sigma_1^{CKG}(\omega)$  [and  $\sigma_1^{KG}(\omega)$  as well; see Sec. IV C].

The continuous Kubo-Greenwood formula, unlike the usual one, gives a direct expression for static electrical conductivity and thermal conductivity.

### B. The limit of zero broadening $\Delta E$

It will be shown here that the continuous Kubo-Greenwood formula (22) is equivalent to the exact one (2) in the limit  $\Delta E \rightarrow 0$ .

First of all, the density of states  $g(\varepsilon)$ , given by Eq. (12), reduces to the sum of exact  $\delta$  functions in the limit  $\Delta E \rightarrow 0$ . Let us denote this limiting function as  $c(\varepsilon)$ :

$$\lim_{\Delta E \rightarrow 0} g(\varepsilon) \equiv c(\varepsilon) = \sum_i \delta(\varepsilon - \varepsilon_i). \quad (29)$$

Let us introduce the notation

$$G_{\omega}(\varepsilon_1, \varepsilon_2) = h(\varepsilon_1, \varepsilon_2) \times \frac{f(\varepsilon_1) - f(\varepsilon_2)}{\hbar\omega} \delta(\varepsilon_2 - \varepsilon_1 - \hbar\omega). \quad (30)$$

Next, consider the sum in expression (2):

$$\sum_i \sum_j G_{\omega}(\varepsilon_i, \varepsilon_j). \quad (31)$$

Each term in (31) can be expressed in an integral form:

$$G_{\omega}(\varepsilon_i, \varepsilon_j) = \iiint G_{\omega}(\varepsilon_1, \varepsilon_2) \times \delta(\varepsilon_1 - \varepsilon_i) \delta(\varepsilon_2 - \varepsilon_j) d\varepsilon_1 d\varepsilon_2. \quad (32)$$

Then (31) can be rewritten as follows:

$$\sum_i \sum_j G_{\omega}(\varepsilon_i, \varepsilon_j) = \iiint G_{\omega}(\varepsilon_1, \varepsilon_2) \times c(\varepsilon_1) c(\varepsilon_2) d\varepsilon_1 d\varepsilon_2. \quad (33)$$

Substituting Eq. (30) into Eq. (33) and performing integration over variable  $\varepsilon_2$ , we obtain the *exact Kubo-Greenwood formula in a “continuous” form*:

$$\sigma_1(\omega) = \frac{2\pi e^2 \hbar^3}{m_e^2 \Omega} \int h(\varepsilon, \varepsilon + \hbar\omega) c(\varepsilon) c(\varepsilon + \hbar\omega) \times \frac{f(\varepsilon) - f(\varepsilon + \hbar\omega)}{\hbar\omega} d\varepsilon. \quad (34)$$

Equation (34) has the same form as the continuous Kubo-Greenwood formula (22). They differ in that functions  $D(\varepsilon_1, \varepsilon_2)$  and  $g(\varepsilon)$  are continuous and smooth, whereas functions  $h(\varepsilon_1, \varepsilon_2)$  and  $c(\varepsilon)$  are not. The last two functions

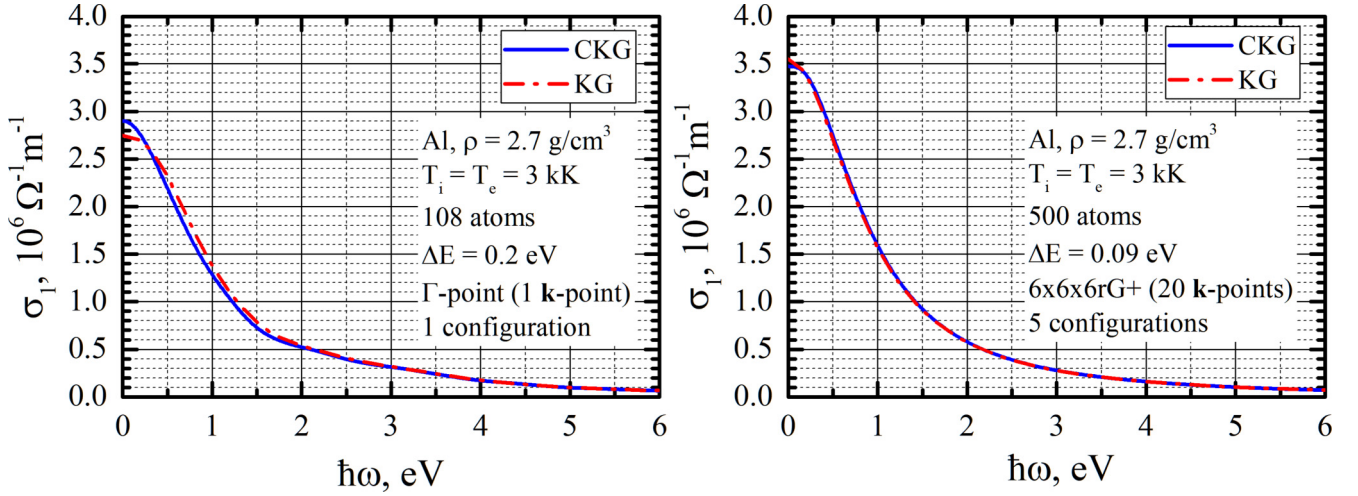


FIG. 3. Comparison of the results obtained using the usual and continuous Kubo-Greenwood formulas. The dash-dotted red curve was calculated by Eq. (5) using GREEKUP, and the solid blue one by Eq. (22) using CUBOGRAM. In both cases (“CKG” and “KG”), the broadening  $\Delta E$  of the  $\delta$  function was chosen to be the same. The calculation was carried out for liquid aluminum at the density  $\rho = 2.7 \text{ g/cm}^3$  and equilibrium temperature of  $T_i = T_e = 3 \text{ kK}$ . The supercell contains 108 atoms (left) and 500 atoms (right).

are nonzero only at eigenvalues  $\varepsilon_i$  and equal to zero at other points.

The continuous Kubo-Greenwood formula (22) will be equivalent to the exact one [Eq. (34)] in the limit  $\Delta E \rightarrow 0$ , if

$$c(\varepsilon) = \lim_{\Delta E \rightarrow 0} g(\varepsilon), \quad (35)$$

$$h(\varepsilon_1, \varepsilon_2) = \lim_{\Delta E \rightarrow 0} D(\varepsilon_1, \varepsilon_2). \quad (36)$$

Equation (35) is just the definition (29) of  $c(\varepsilon)$ . Let us turn to expression (16). If  $(\varepsilon_1, \varepsilon_2) = (\varepsilon_i, \varepsilon_j)$  for some  $(i, j)$ , only one matrix element squared  $D_{ij}$  is contained inside  $\Pi$  in the limit  $\Delta E \rightarrow 0$ :

$$D(\varepsilon_i, \varepsilon_j)|_{\Delta E \rightarrow 0} = \frac{D_{ij} \times \frac{1}{2\Delta E} \times \frac{1}{2\Delta E}}{\frac{1}{2\Delta E} \times \frac{1}{2\Delta E}} = h(\varepsilon_i, \varepsilon_j). \quad (37)$$

If  $(\varepsilon_1, \varepsilon_2) \neq (\varepsilon_i, \varepsilon_j)$ , the function  $D(\varepsilon_1, \varepsilon_2)$  is undefined in the limit  $\Delta E \rightarrow 0$  (indeterminate form 0/0). Let us redefine it by zero in this case; this will have no effect on the value of the integral in Eq. (22). That proves relation (36).

Thus, we get that both the continuous [Eq. (22)] and usual [Eq. (5)] Kubo-Greenwood formulas reduce to the exact one [Eq. (2)] in the limit of zero broadening,  $\Delta E \rightarrow 0$ . Hence, we treat the continuous Kubo-Greenwood formula as an alternative method for calculating the real part of dynamic electrical conductivity.

### C. Finite broadening $\Delta E$

It was shown that the calculations of the conductivity by the usual and continuous Kubo-Greenwood formulas [ $\sigma_1^{KG}(\omega)$  and  $\sigma_1^{CKG}(\omega)$ , respectively] are equivalent only in the limit of infinitely small broadening  $\Delta E$ .

Here, we will show that even at finite  $\Delta E$  these formulas still give close results. To do this, we calculate the curves  $\sigma_1^{KG}(\omega)$  and  $\sigma_1^{CKG}(\omega)$  for the system described in Sec. V. The technical parameters of the computation are specified in Sec. VIA. The results are shown in Fig. 3 (right). The

difference between the curves  $\sigma_1^{KG}(\omega)$  and  $\sigma_1^{CKG}(\omega)$  is no more than 2% for all frequencies  $\omega$ .

However, the difference increases for a smaller number of atoms in a supercell. To illustrate this, a similar calculation is performed with 108 atoms in the supercell. Only the  $\Gamma$  point is used during the QMD simulation and band structure calculation. Electrical conductivity is calculated only for the last ionic configuration from the equilibrium section of the QMD simulation; 300 and 500 bands are taken into account during the QMD simulation and band structure calculation, respectively. The broadening  $\Delta E$  is 0.2 eV. Other simulation parameters are the same as in Sec. VIA. The results of this calculation are shown in Fig. 3 (left). The difference is no more than 13% along the entire curve.

Thus, both calculation methods give fairly close conductivity results. Therefore, the analysis of the contributions to  $\sigma_1^{CKG}(\omega)$  explains how the conductivity curve  $\sigma_1^{CKG}(\omega)$  is formed.

## V. EXAMPLE OF CALCULATION ACCORDING TO THE CONTINUOUS KUBO-GREENWOOD FORMULA

In this section, we show an example of practical calculation of  $\sigma_{1DC}^{CKG}$  and  $L_{22}^{CKG}$  using the continuous Kubo-Greenwood formula (26). The system under consideration is liquid aluminum at a density  $\rho = 2.7 \text{ g/cm}^3$  and temperature  $T_e = T_i = 3 \text{ kK}$ . Technical computation parameters are given in Sec. VIA.

We are mostly interested in the functions  $D(\varepsilon, \varepsilon)\Omega$ ,  $g^2(\varepsilon)/\Omega^2$ ,  $-\partial f/\partial \varepsilon(\varepsilon)$ , and  $(\varepsilon - \mu)^2$ . They make up contributions to  $\sigma_{1DC}^{CKG}$  and  $L_{22}^{CKG}$  in Eq. (26). These contributions (and their products) calculated for the system under consideration are shown in Fig. 4.

Several graphs are shown in Fig. 4 with the same energy axis: DOS per unit volume  $g(\varepsilon)/\Omega$  and the Fermi-Dirac distribution  $f(\varepsilon)$  [Fig. 4(a)]; SSME multiplied by the volume of the supercell  $D(\varepsilon, \varepsilon)\Omega$  [Fig. 4(b)]; the square of DOS per unit volume  $g^2(\varepsilon)/\Omega^2$  [Fig. 4(c)]; the derivative of the Fermi-Dirac

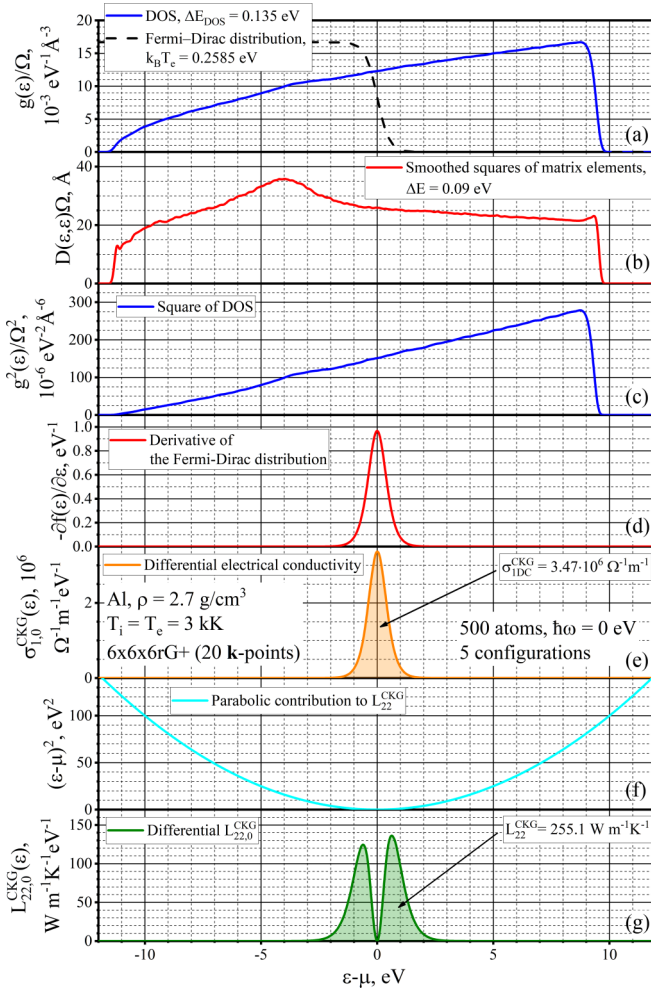


FIG. 4. Contributions to electrical and thermal conductivities. Areas under the graph in (e) and (g) are the values of  $\sigma_{1DC}^{CKG}$  and  $L_{22}^{CKG}$ , respectively.

distribution with a minus sign  $-\partial f/\partial \varepsilon(\varepsilon)$  [Fig. 4(d)]; the differential static electrical conductivity  $\sigma_{1,0}^{CKG}(\varepsilon)$  [Fig. 4(e)], which is obtained by multiplying the graphs in Figs. 4(b)–(d) (up to a constant factor); the parabolic contribution  $(\varepsilon - \mu)^2$  [Fig. 4(f)]; and the differential thermal conductivity  $L_{22,0}^{CKG}(\varepsilon)$  [Fig. 4(g)], which is obtained by multiplying the graphs in Figs. 4(b)–(d) and 4(f) (up to a constant factor). By analyzing these contributions one could understand how the electrical static  $\sigma_{1DC}^{CKG}$  and thermal  $L_{22}^{CKG}$  conductivities are formed.

One can see that  $D(\varepsilon, \varepsilon)\Omega$  is almost constant around  $\varepsilon = \mu$ . At the same time  $g^2(\varepsilon)/\Omega^2$  behaves linearly. The derivative of the Fermi-Dirac distribution is bell shaped, symmetric, and centered on  $\varepsilon = \mu$ . The area under  $-\partial f/\partial \varepsilon(\varepsilon)$  is unity and we introduce the width of this curve as inverse value at maximum. Thus the width is  $4k_B T_e$  and the half width is  $2k_B T_e$ . The product of these three curves forms the differential electrical conductivity; multiplying it by  $(\varepsilon - \mu)^2$  forms the  $L_{22,0}^{CKG}(\varepsilon)$  curve. Numerical integration of these dependencies gives the values of  $\sigma_{1DC}^{CKG}$  and  $L_{22}^{CKG}$ :

$$\sigma_{1DC}^{CKG} = 3.47 \times 10^6 \frac{1}{\Omega \mu}, \quad L_{22}^{CKG} = 255.1 \frac{W}{m K}. \quad (38)$$

For comparison, here are the values obtained using the GREEKUP code [39] via the usual Kubo-Greenwood formula (6):

$$\sigma_{1DC}^{KG} = 3.55 \times 10^6 \frac{1}{\Omega \mu}, \quad L_{22}^{KG} = 262.7 \frac{W}{m K}. \quad (39)$$

The differences are no more than 3%.

The prominent feature of Fig. 4 is the part of the spectrum contributing mostly to  $\sigma_{1DC}^{CKG}$  and  $L_{22}^{CKG}$ : a rather narrow stripe around chemical potential  $\mu$ . A similar idea is discussed for solid state at low temperatures in the book of Ashcroft and Mermin (pp. 53 and 250 of [42]). However, in our previous papers employing the usual KG formula [35,40,43], it was a rather hard task to strictly prove even this well-known idea. The only quantities we could operate were the values of  $\sigma_{1DC}$  and the curves  $g(\varepsilon)/\Omega$ ,  $-\partial f/\partial \varepsilon(\varepsilon)$ . In fact, using this incomplete information we could present rather speculative arguments about the part of the spectrum mostly contributing to electrical conductivity (see Fig. 7 of [43]). The situation changes drastically if we introduce the continuous Kubo-Greenwood formula. Now we have the smooth differential electrical conductivity  $\sigma_{1,0}^{CKG}(\varepsilon)$  [Fig. 4(e)]; the integral of this function yields the correct value  $\sigma_{1DC}^{CKG} \approx \sigma_{1DC}^{KG}$ . Thus we can quantitatively determine what percentage of a final  $\sigma_{1DC}^{CKG}$  value is due to each part of the spectrum. We treat the possibility of such an analysis as a distinct advantage of the continuous Kubo-Greenwood formula.

## VI. TECHNICALITIES

### A. Technical parameters

In our previous paper [35], we explain how we choose technical parameters during QMD simulation, detailed calculation of the band structure, and computation via the usual KG formula. There, we discuss many questions connected with the influence of technical parameters and convergence.

In this section, we provide all technical parameters used in the current paper. The presence of two broadenings simultaneously,  $\Delta E$  and  $\Delta E_{DOS}$ , is the peculiarity of a calculation via the continuous Kubo-Greenwood formula. We discuss the influence of these parameters and their optimal choice in Secs. VI B and VI C.

In this paper, QMD simulation was performed for 500 atoms of Al in the cubic supercell with periodic boundary conditions. The supercell volume  $\Omega$  was chosen to obtain  $\rho = 2.7 \text{ g/cm}^3$ . Ion and electron temperatures are equal:  $T_i = T_e = 3 \text{ kK}$ . At the initial moment of QMD simulation ions are placed in fcc positions. The evolution of the system during 4 ps was simulated with a 2-fs time step. The pseudopotential of the projector augmented-wave (PAW) type [44] with three valence electrons is used. The Perdew-Burke-Ernzerhof (PBE) parametrization [45] from the generalized gradient approximation (GGA) class is used as an exchange-correlation (XC) functional. All plane waves with a kinetic energy smaller than  $E_{cut} = 200 \text{ eV}$  are included in the basis set. Only a  $\Gamma$  point in the Brillouin zone is used. We ensure that all bands with occupation numbers greater than  $2.5 \times 10^{-6}$  are taken into account during the QMD simulation; this yields  $N_{bands} = 1300$ .



The calculation of optical and transport properties requires more precise electron structure determination. Hence, five ionic configurations are chosen from the range  $3.2 \leq t_s \leq 4$  ps; the system reaches equilibrium before this period. For these configurations the band structure is computed with the same pseudopotential, XC functional, and  $E_{\text{cut}}$ . The reduced  $\Gamma$ -centered  $6 \times 6 \times 6$  Monkhorst-Pack grid (20  $\mathbf{k}$  points) is used (see Secs. A.1 and A.2 of [35]). Additional 600 bands were taken into account to calculate  $\sigma_1(\omega)$  up to  $\hbar\omega_{\text{max}} = 6$  eV.

Broadening  $\Delta E$  is 0.09 eV and broadening during the calculation of DOS is  $\Delta E_{\text{DOS}} = 1.5 \times \Delta E = 0.135$  eV. In this work the Gaussian broadening (40) is used in all numerical computations. Optical matrix elements squared  $D_{ij}^{\mathbf{k}}$  are obtained by the LO-L method (Sec. VID 1 d). Computed quantities are averaged over five chosen ionic configurations.

Since we use a rather large number of atoms and  $\mathbf{k}$  points, the curves  $D(\varepsilon, \varepsilon)$  and  $g(\varepsilon)$  are fairly smooth even for one ionic configuration. Averaging over five ionic configurations has a weak effect. Thus, we consider five ionic configurations to be enough; further increase would be time-consuming and have negligible effect. In our previous paper (see Sec. 3.4 of [35]), we have found out that, in similar conditions, the increase of  $E_{\text{cut}}$  from 200 to 400 eV changes the value of  $\sigma_{\text{IDC}}^{\text{CKG}}$  by less than 1%. Further increase of the number of  $\mathbf{k}$  points (from 20 to 35) leads to an insignificant change of  $\sigma_{\text{IDC}}^{\text{CKG}}$  (less than 0.1%).

In the following sections we consider the influence of the technical parameters: the relationship between  $\Delta E$  and  $\Delta E_{\text{DOS}}$  (Sec. VIB), the broadening  $\Delta E$  (Sec. VIC), and the method of calculating matrix elements (Sec. VID).

In Secs. VIB and VIC we will change only parameters  $\Delta E$  and  $\Delta E_{\text{DOS}}$ , keeping the others same as above.

In Sec. VID we use only the Baldereschi  $\mathbf{k}$  point (0.25, 0.25, 0.25) during the second stage of computation and vary the method of calculating matrix elements. Different pseudopotential and XC functional are also used if matrix elements are calculated by the GKP method (Sec. VID 1 a).

### B. The relationship between $\Delta E$ and $\Delta E_{\text{DOS}}$

The broadened  $\delta$  functions are used to calculate DOS (12) and SSME (16). In Sec. III A a rectangle broadening (11) is used during the theoretical consideration. In practice one can use different types of broadening. In this work, we prefer the Gaussian broadening in all computations:

$$\delta_{\Delta E}(\varepsilon - \varepsilon_i) = \frac{1}{\sqrt{2\pi}\Delta E} \exp\left[-\frac{(\varepsilon - \varepsilon_i)^2}{2(\Delta E)^2}\right]. \quad (40)$$

The Gaussian broadening has a number of advantages. First, it yields smoother DOS and SSME. Second, it allows to resolve automatically the indeterminate form we discussed in Sec. IV B; we will consider this question below.

Note that unequal values of  $\Delta E$  and  $\Delta E_{\text{DOS}}$  could be used in the numerator and denominator of Eq. (16), respectively. The relationship between  $\Delta E$  and  $\Delta E_{\text{DOS}}$  affects the computation of  $D(\varepsilon_1, \varepsilon_2)$ , if the Gaussian broadening is used.

Let us perform a model consideration for only one nonzero matrix element squared  $B = |\langle \Psi_0 | \nabla | \Psi_0 \rangle|^2 = |D_{00}|^2$  to illustrate this. Let the energy eigenvalue corresponding to the state  $|\Psi_0\rangle$  be  $\varepsilon_0$ . Let us calculate the function  $D(\varepsilon, \varepsilon)$  (up to a

constant factor):

$$\begin{aligned} D(\varepsilon, \varepsilon) &\propto \frac{B \exp\left[-\frac{(\varepsilon - \varepsilon_0)^2}{(\Delta E)^2}\right]}{\exp\left[-\frac{(\varepsilon - \varepsilon_0)^2}{(\Delta E_{\text{DOS}})^2}\right]} \\ &= B \exp\left[-(\varepsilon - \varepsilon_0)^2 \left(\frac{1}{(\Delta E)^2} - \frac{1}{(\Delta E_{\text{DOS}})^2}\right)\right]. \end{aligned} \quad (41)$$

If  $\Delta E_{\text{DOS}} = \Delta E$ ,

$$D(\varepsilon, \varepsilon) \propto B e^{-(\varepsilon - \varepsilon_0)^2 \times 0} = B = \text{const.} \quad (42)$$

If  $\Delta E_{\text{DOS}} < \Delta E$ ,

$$D(\varepsilon, \varepsilon) \propto B e^{(\varepsilon - \varepsilon_0)^2 \left|\frac{1}{(\Delta E)^2} - \frac{1}{(\Delta E_{\text{DOS}})^2}\right|} \xrightarrow{|\varepsilon - \varepsilon_0| \rightarrow \infty} \infty. \quad (43)$$

If  $\Delta E_{\text{DOS}} > \Delta E$ ,

$$D(\varepsilon, \varepsilon) \propto B e^{-(\varepsilon - \varepsilon_0)^2 \left|\frac{1}{(\Delta E)^2} - \frac{1}{(\Delta E_{\text{DOS}})^2}\right|} \xrightarrow{|\varepsilon - \varepsilon_0| \rightarrow \infty} 0. \quad (44)$$

This model theoretical consideration helps to understand the numerical results (Fig. 5). The different shapes of  $D(\varepsilon, \varepsilon)$  at the spectrum edge are created by purely numerical effects. The cases  $\Delta E = \Delta E_{\text{DOS}}$  and  $\Delta E > \Delta E_{\text{DOS}}$  lead to the nonphysical behavior of  $D(\varepsilon, \varepsilon)$  beyond the spectrum range. We observe nonzero values of the transition intensity in the energy range where there are no initial states (or where bands were not taken into account during the electron structure calculation). If  $\Delta E = \Delta E_{\text{DOS}}$  there is no well-pronounced plateau in Fig. 5 (blue curve). However, more realistic consideration of several matrix elements could explain the complex (and still nonphysical) behavior of  $D(\varepsilon, \varepsilon)$  beyond the spectrum range in this case. We also observe that in the region of nonzero  $g(\varepsilon)$ , the functions  $D(\varepsilon, \varepsilon)$  are nearly the same in all cases.

Thus, when implementing the  $D(\varepsilon_1, \varepsilon_2)$  calculation using the Gaussian broadening, it is required to comply with the condition  $\Delta E_{\text{DOS}} > \Delta E$ . Also, this relationship of broadenings leads to more numerically stable results. If  $\Delta E_{\text{DOS}} > \Delta E$ , the ratio  $\Delta E_{\text{DOS}}/\Delta E$  should not be too close to 1; in this paper, we set this ratio to 1.5.

Due to the multiplication of the function  $D(\varepsilon_1, \varepsilon_2)$  by  $g(\varepsilon_1)g(\varepsilon_2)$  in Eq. (22), the final value of conductivity  $\sigma_1^{\text{CKG}}(\omega)$  depends only on  $\Delta E$ , but not on  $\Delta E_{\text{DOS}}$ .

### C. Dependence on the broadening $\Delta E$

The broadening of the  $\delta$  function,  $\Delta E$ , is an important parameter of SSME calculation by Eq. (16). Ideally, the broadening of the  $\delta$  function should be much less than any characteristic value of energy considered in the problem. In our case, particularly, one needs to require  $\Delta E \ll 2k_B T_e$ . However, it may be rather difficult to satisfy this condition. Often one has to choose  $\Delta E < 2k_B T_e$ , but not  $\Delta E \ll 2k_B T_e$ .

We also investigate numerically the influence of  $\Delta E$  on  $D(\varepsilon, \varepsilon)$  and  $g(\varepsilon)$  to select the optimal value of this parameter. These functions were calculated for the same system as described in Sec. V. The ratio  $\Delta E_{\text{DOS}}/\Delta E = 1.5$  is kept constant. The calculation results are shown in Fig. 6.

If the broadening is too small, considerable oscillations emerge on the curves ( $\Delta E = 0.02$  eV,  $\Delta E_{\text{DOS}} = 0.03$  eV, red curve). At a comparatively large broadening the function

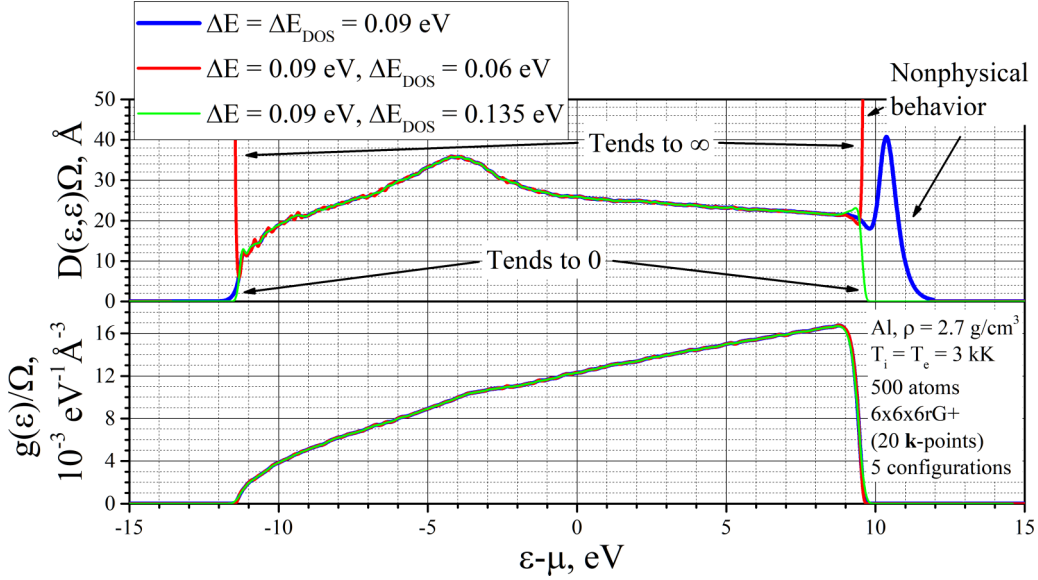


FIG. 5. The behavior of SSME  $D(\varepsilon, \varepsilon)\Omega$  for different relationships between  $\Delta E$  and  $\Delta E_{DOS}$  in the case of the Gaussian broadening. DOS  $g(\varepsilon)/\Omega$  is also reported to represent the boundaries of the electron spectrum. If  $\Delta E_{DOS} = \Delta E$  (blue curve), nonzero values of  $D(\varepsilon, \varepsilon)$  appear beyond the spectrum range. If  $\Delta E_{DOS} < \Delta E$  (red curve), the function tends to infinity at the spectrum boundaries. If  $\Delta E > \Delta E_{DOS}$ , the function exponentially decreases to zero at the spectrum edges. The last condition is used during the calculation (Sec. VI A).

$D(\varepsilon, \varepsilon)$  is underestimated ( $\Delta E = 0.2$  eV,  $\Delta E_{DOS} = 0.3$  eV, green curve). The optimal broadening value can be chosen as  $\Delta E = 0.09$  eV (black curve).

In this work, we consider  $k_B T_e = 0.26$  eV. For the selected broadenings  $\Delta E_{DOS}/(2k_B T_e) = 0.26$ ,  $\Delta E/(2k_B T_e) = 0.17$ . Thus, both  $\Delta E_{DOS}$  and  $\Delta E$  are several times less than  $2k_B T_e$ .

It is also worth noting that in the case of DOS, when the broadening is varied, the area under the graph  $g(\varepsilon)$  is preserved. In the case of  $D(\varepsilon_1, \varepsilon_2)$ , the volume under the surface  $D_g(\varepsilon_1, \varepsilon_2) = D(\varepsilon_1, \varepsilon_2)g(\varepsilon_1)g(\varepsilon_2)$  is preserved. That is why the area under the  $D(\varepsilon, \varepsilon)$  curve does not remain constant when the broadening is changed.

#### D. Dependence on the method of calculating of matrix elements

At the second stage of calculation we obtain information on electronic structure, including energy eigenvalues and wave functions. Then this information is used to compute matrix elements squared  $D_{ij}^k$ , which are necessary to calculate transport and optical properties. A number of technical details should be mentioned here.

First, the pseudopotential approach is used in the VASP package. The generalized Kohn-Sham equations on pseudowave functions  $|\tilde{\Psi}_{i,k}\rangle$  are solved instead of the usual Kohn-Sham equations on all-electron wave functions  $|\Psi_{i,k}\rangle$  [38,44]. These pseudowave functions even do not have to be orthonormal, in contrast to all-electron ones. The matrix

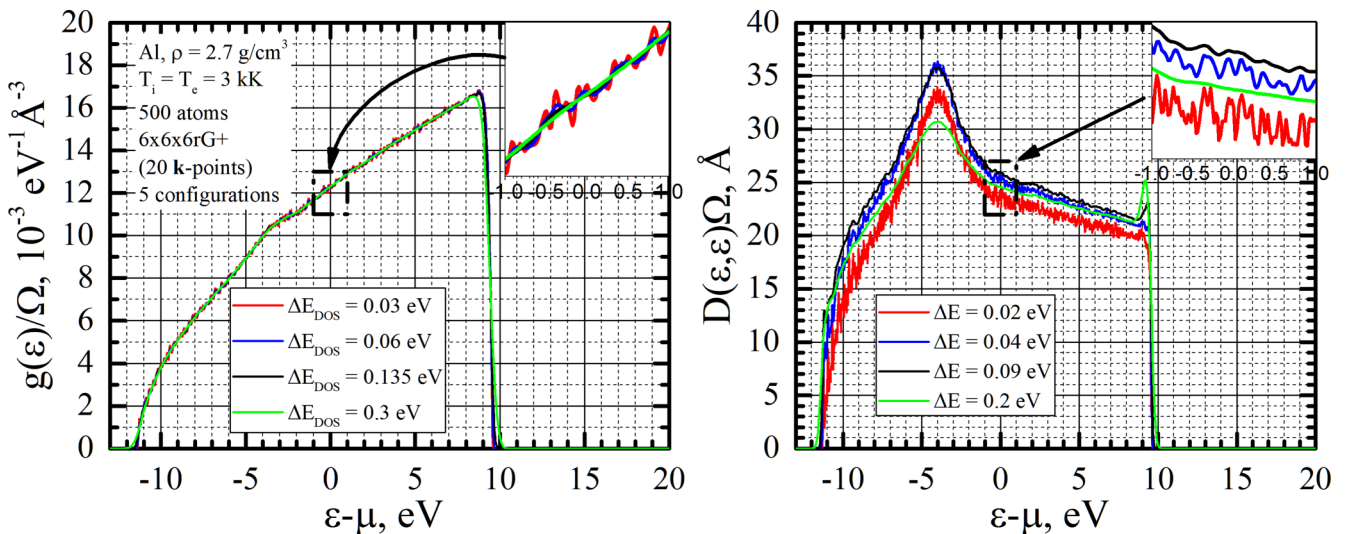


FIG. 6. Dependence of DOS (left) and SSME (right) on the broadening of the  $\delta$  function,  $\Delta E$ . The ratio  $\Delta E_{DOS}/\Delta E = 1.5$  is conserved. The corresponding curves  $g(\varepsilon)/\Omega$  and  $D(\varepsilon, \varepsilon)\Omega$  have the same color.

elements cannot be calculated from pseudowave functions, available in VASP, just as  $\langle \tilde{\Psi}_{i,\mathbf{k}} | \nabla_\alpha | \tilde{\Psi}_{j,\mathbf{k}} \rangle$ ; the conversion to  $\langle \Psi_{i,\mathbf{k}} | \nabla_\alpha | \Psi_{j,\mathbf{k}} \rangle$  should be performed.

Second, “transverse” and “longitudinal” formulas for dynamic electrical conductivity (and dielectric function) exist [46]. These two formulas include different matrix elements. Both formulas are valid if local potentials are considered, but only the longitudinal formula provides the correct treatment of nonlocal potentials. Some other differences between numerical implementations of the transverse and longitudinal formulas exist even for local potentials (see the end of Sec. II B of [46]). The matrix elements for the transverse formula are calculated in two different source files of VASP.

Hence, it turns out that different matrix elements squared  $D_{ij}^{\mathbf{k}}$  can be obtained using VASP. Below, in Sec. VID 1 we briefly describe four methods of calculating  $D_{ij}^{\mathbf{k}}$ . In Sec. VID 2 we compare the functions  $D(\varepsilon, \varepsilon)$  and  $\sigma_1^{CKG}(\omega)$  obtained using these four methods.

### 1. Methods of calculating matrix elements

*a. Ultrasoft pseudopotential (GKP).* In the first method the ultrasoft pseudopotential (US) [47] is used. We have shown numerically that one of the US pseudopotentials for Al supplied with the VASP package ensures the valid orthonormality condition for pseudowave functions:

$$\langle \tilde{\Psi}_{i,\mathbf{k}} | \tilde{\Psi}_{j,\mathbf{k}} \rangle = \delta_{ij}. \quad (45)$$

Here  $\delta_{ij}$  is the Kronecker delta. Then it is interesting to use matrix elements  $\langle \tilde{\Psi}_{i,\mathbf{k}} | \nabla_\alpha | \tilde{\Psi}_{j,\mathbf{k}} \rangle$  for this pseudopotential directly, without the conversion to the all-electron wave functions. Thus, we obtain the following expression for  $D_{ij}^{\mathbf{k}}$ :

$$D_{ij}^{\mathbf{k}} = \frac{1}{3} \sum_{\alpha} |\langle \tilde{\Psi}_{i,\mathbf{k}} | \nabla_\alpha | \tilde{\Psi}_{j,\mathbf{k}} \rangle|^2. \quad (46)$$

This calculation of such matrix elements is performed using the GREEKUP code [39] and will be further marked with the “GKP” tag. Note that the Perdew-Zunger parametrization [48] from the local density approximation (LDA) class is used as an XC functional during the GKP calculation.

In the following three methods, the PAW pseudopotential is used [44].

*b. optics.F (OPT).* Here, the conversion from  $\langle \tilde{\Psi}_{i,\mathbf{k}} | \nabla_\alpha | \tilde{\Psi}_{j,\mathbf{k}} \rangle$  to  $\langle \Psi_{i,\mathbf{k}} | \nabla_\alpha | \Psi_{j,\mathbf{k}} \rangle$  for the PAW pseudopotential (see Eq. (5) of [49]) is performed. Thus,

$$D_{ij}^{\mathbf{k}} = \frac{1}{3} \sum_{\alpha} |\langle \Psi_{i,\mathbf{k}} | \nabla_\alpha | \Psi_{j,\mathbf{k}} \rangle|^2. \quad (47)$$

Such a calculation of matrix elements is performed using the serial algorithm of the VASP program implemented in the source file optics.F. Calculation of this type will be further marked with the “OPT” tag.

*c. Transverse formula (LO-T).* Let us consider the calculation of the real part of dynamic electrical conductivity (or imaginary part of dielectric function) according to the “transverse” formula (see Eq. (18) of [46]). Matrix elements of the operator  $i\nabla_\alpha - \mathbf{k}_\alpha$  between the two Bloch functions  $|u_{i,\mathbf{k}}\rangle$  are present in this formula. These matrix elements are calculated via a parallel algorithm implemented in the

source file linear\_optics.F (and nested subroutines). Using  $|\Psi_{j,\mathbf{k}}\rangle = e^{i\mathbf{k}\mathbf{r}}|u_{j,\mathbf{k}}\rangle$ , one can find

$$\langle u_{i,\mathbf{k}} | i\nabla_\alpha - \mathbf{k}_\alpha | u_{j,\mathbf{k}} \rangle = i \langle \Psi_{i,\mathbf{k}} | \nabla_\alpha | \Psi_{j,\mathbf{k}} \rangle. \quad (48)$$

In this case, we obtain the same theoretical expression for  $D_{ij}^{\mathbf{k}}$  as for the OPT method (47):

$$\begin{aligned} D_{ij}^{\mathbf{k}} &= \frac{1}{3} \sum_{\alpha} |\langle u_{i,\mathbf{k}} | i\nabla_\alpha - \mathbf{k}_\alpha | u_{j,\mathbf{k}} \rangle|^2 \\ &= \frac{1}{3} \sum_{\alpha} |\langle \Psi_{i,\mathbf{k}} | \nabla_\alpha | \Psi_{j,\mathbf{k}} \rangle|^2. \end{aligned} \quad (49)$$

Thus, the result of this calculation is expected to be the same as for the OPT method.

This type of computation will be further marked with the “LO-T” tag.

*d. Longitudinal formula (LO-L).* Let us consider the calculation of the real part of dynamic electrical conductivity according to the “longitudinal” formula (see Eq. (15) of [46]). The matrix elements  $\langle u_{i,\mathbf{k}} | \partial u_{j,\mathbf{k}} / \partial k_\alpha \rangle$  are present in this formula. These matrix elements are calculated using a parallel algorithm implemented in the source file linear\_optics.F (and nested subroutines). One could find that

$$\begin{aligned} -i \left\langle u_{i,\mathbf{k}} \left| \frac{\partial u_{j,\mathbf{k}}}{\partial k_\alpha} \right. \right\rangle &= -\langle u_{i,\mathbf{k}} | \hat{r}_\alpha | u_{j,\mathbf{k}} \rangle \\ &= -\langle \Psi_{i,\mathbf{k}} | \hat{r}_\alpha | \Psi_{j,\mathbf{k}} \rangle, \end{aligned} \quad (50)$$

where  $\hat{r}_\alpha$  is the coordinate operator.

We multiply the matrix elements (50) calculated in linear\_optics.F by  $-m_e(\varepsilon_{j,\mathbf{k}} - \varepsilon_{i,\mathbf{k}})/\hbar^2$ . This makes them applicable in formulation (2) of the Kubo-Greenwood formula present in our paper. Thus, we obtain

$$\begin{aligned} D_{ij}^{\mathbf{k}} &= \frac{1}{3} \frac{m_e^2}{\hbar^4} (\varepsilon_{j,\mathbf{k}} - \varepsilon_{i,\mathbf{k}})^2 \sum_{\alpha} |\langle \Psi_{i,\mathbf{k}} | \hat{r}_\alpha | \Psi_{j,\mathbf{k}} \rangle|^2 \\ &= \frac{1}{3} \frac{m_e^2}{\hbar^4} (\varepsilon_{j,\mathbf{k}} - \varepsilon_{i,\mathbf{k}})^2 \sum_{\alpha} \left| \left\langle u_{i,\mathbf{k}} \left| \frac{\partial u_{j,\mathbf{k}}}{\partial k_\alpha} \right. \right\rangle \right|^2. \end{aligned} \quad (51)$$

This works as follows. If one substitutes Eq. (51) into Eq. (2), the longitudinal formula (Eq. (15) of [46]) is obtained. If we run the GREEKUP code with the matrix elements (51), we obtain the valid numerical implementation of the longitudinal formula. The calculation according to the continuous Kubo-Greenwood formula (16) and (22) via the CUBOGRAM code with  $D_{ij}^{\mathbf{k}}$  given by Eq. (51) is another numerical implementation of the longitudinal formula. Calculation of this type will be further marked with the “LO-L” tag.

The relationship between this method and the methods OPT and LO-T can be shown better if we consider the connection between the matrix elements of coordinate  $\hat{r}_\alpha$  and gradient  $\nabla_\alpha$  operators:

$$\begin{aligned} \langle \Psi_{i,\mathbf{k}} | \nabla_\alpha - \frac{m_e}{\hbar^2} [\hat{V}, \hat{r}_\alpha] | \Psi_{j,\mathbf{k}} \rangle \\ = \frac{m_e}{\hbar^2} (\varepsilon_{j,\mathbf{k}} - \varepsilon_{i,\mathbf{k}}) \langle \Psi_{i,\mathbf{k}} | \hat{r}_\alpha | \Psi_{j,\mathbf{k}} \rangle. \end{aligned} \quad (52)$$

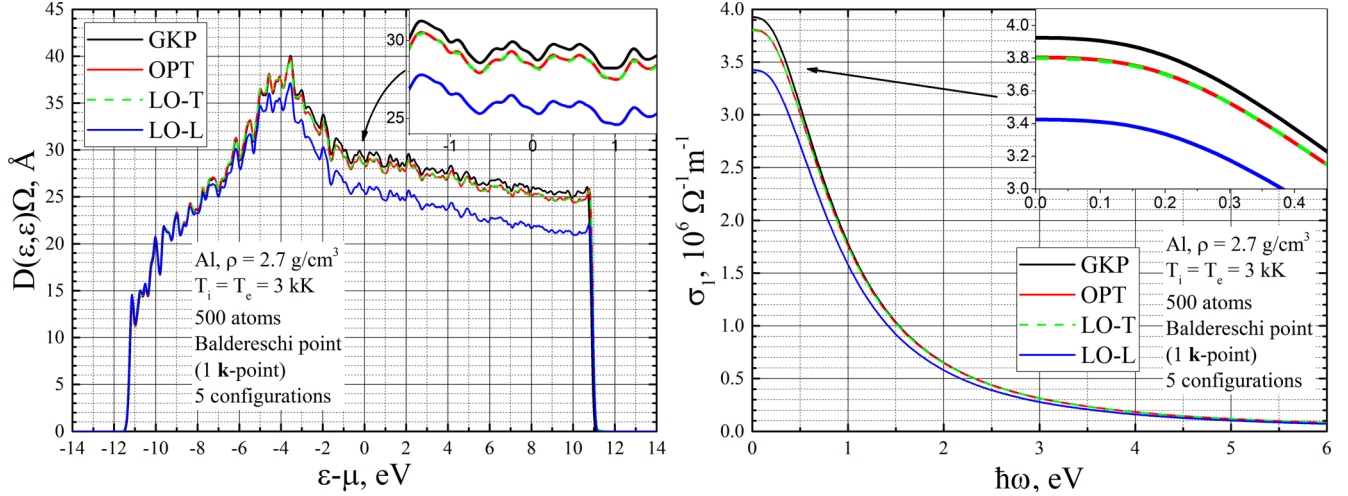


FIG. 7. SSME for the static case  $D(\varepsilon, \varepsilon)\Omega$  (left) and electrical conductivity  $\sigma_1^{CKG}(\omega)$  (right) for all methods of calculating matrix elements. OPT and LO-T calculations gave very close results. GKP curves are situated only a bit higher than LO-T ones. The LO-L values are significantly lower than those obtained by the LO-T method.

Here,  $\hat{V}$  is the effective potential in the Kohn-Sham equations. The derivation of relationship (52) can be found in our earlier paper (see Eq. (16) of [39]).

If potential  $\hat{V}$  is local, it commutes with  $\hat{r}_\alpha$ :  $[\hat{V}, \hat{r}_\alpha] = 0$ . In this case Eq. (51) reduces to

$$\begin{aligned} D_{ij}^k &= \frac{1}{3} \frac{m_e^2}{\hbar^4} (\varepsilon_{j,\mathbf{k}} - \varepsilon_{i,\mathbf{k}})^2 \sum_{\alpha} |\langle \Psi_{i,\mathbf{k}} | \hat{r}_\alpha | \Psi_{j,\mathbf{k}} \rangle|^2 \\ &= \frac{1}{3} \sum_{\alpha} |\langle \Psi_{i,\mathbf{k}} | \nabla_{\alpha} | \Psi_{j,\mathbf{k}} \rangle|^2. \end{aligned} \quad (53)$$

Therefore, in case of a local potential the LO-L method theoretically should give the same results as the LO-T (and OPT) methods. However, some discrepancy with the LO-T method is still possible due to the features of the VASP code (see the end of Sec. II B of [46]).

If the potential  $\hat{V}$  is nonlocal, the necessary corrections are taken into account in the LO-L method. This follows from Eqs. (51) and (52):

$$\begin{aligned} D_{ij}^k &= \frac{1}{3} \frac{m_e^2}{\hbar^4} (\varepsilon_{j,\mathbf{k}} - \varepsilon_{i,\mathbf{k}})^2 \sum_{\alpha} |\langle \Psi_{i,\mathbf{k}} | \hat{r}_\alpha | \Psi_{j,\mathbf{k}} \rangle|^2 \\ &= \frac{1}{3} \sum_{\alpha} |\langle \Psi_{i,\mathbf{k}} | \nabla_{\alpha} - \frac{m_e}{\hbar^2} [\hat{V}, \hat{r}_\alpha] | \Psi_{j,\mathbf{k}} \rangle|^2. \end{aligned} \quad (54)$$

These corrections are not possible in the OPT method (see Sec. 3.2 of [39]), and are actually taken into account in the LO-L method.

Our previous calculations were performed using the GKP method for aluminum [35,40] and the OPT method for other materials [39]. In this paper all calculations were performed using the LO-L method, unless otherwise specified.

## 2. Results obtained using various methods

Here, we will compare the results obtained using various methods of calculating matrix elements.

The calculation is performed for the same system as in Sec. V. Technical computation parameters are the same as

in Sec. VIA except for  $\mathbf{k}$ -point mesh at the second stage of the calculation. We were able to obtain the OPT curve with only one  $\mathbf{k}$  point since matrix elements are calculated via the serial algorithm. Therefore, all curves in this section are calculated using only one  $\mathbf{k}$  point. We use the Baldereschi  $\mathbf{k}$  point (0.25, 0.25, 0.25) that yields rather smooth results.

Figure 7 demonstrates  $D(\varepsilon, \varepsilon)$  and  $\sigma_1^{CKG}(\omega)$  for all methods of calculating matrix elements.

As expected OPT and LO-T results are almost the same. There are some  $D_{ij}$  that are zero in LO-T but nonzero in OPT computation. It causes a 1% difference in  $D(\varepsilon, \varepsilon)$  between these methods at some energy values; the static conductivity  $\sigma_{IDC}^{CKG}$  differs by 0.1%. Because of that we consider that these methods yield very close but not equal results.

We use the GGA-PBE XC functional during the calculation via OPT, LO-T, and LO-L methods. This local XC functional produces the local effective potential in the Kohn-Sham equations. Therefore, methods LO-T and LO-L should give the same results (Sec. VID 1 d). However, we observe a significant difference between these methods on SSME and  $\sigma_1^{CKG}(\omega)$  graphs. We attribute this discrepancy to the features of calculations mentioned in the paper of Gajdoš *et al.* (see the end of Sec. II B of [46]). Curves  $D(\varepsilon, \varepsilon)$  and  $\sigma_1^{CKG}(\omega)$  for the LO-L calculation are situated below LO-T; the difference in  $\sigma_{IDC}^{CKG}$  is 11%.

The GKP method yields a bit higher results than OPT (and LO-T). However, GKP differs from LO-T less than LO-L differs from LO-T; the difference in  $\sigma_{IDC}^{CKG}$  is 3%.

In paper [46] the similar arrangement of LO-T and LO-L curves (for dielectric function) was obtained for other materials.

Thus, four various methods of matrix elements calculation give noticeably different results. Our technique based on the smoothing procedure and the continuous Kubo-Greenwood formula reveals additional details: using SSME we explicitly analyze the contribution of matrix elements to dynamic electrical conductivity. Hence our approach can provide better understanding of transport properties for more complicated materials.

## VII. RELATED IDEAS IN PREVIOUS WORKS

Here we are going to consider some previous works with related ideas and estimate the contribution of our paper.

The expressions that look like the continuous Kubo-Greenwood formula (22) are present in a number of works [50–56]. While considering these works, one should remember that the continuous KG formula (22) and the exact KG formula in the continuous form (34) look alike but still have different meanings. Equation (22) includes the expressions calculated using broadened  $\delta$  functions, whereas Eq. (34) uses exact  $\delta$  functions. Also, in theoretical works, it is often not stated explicitly whether a continuous or discrete spectrum is considered; sometimes, one may infer that the authors implied the transfer between the two. In our numerical calculations, we obtain a discrete spectrum with small but finite distances between energy levels. The theoretical transfer to a continuous spectrum is not achieved in numerical calculation. In order to get a smooth function  $D(\varepsilon_1, \varepsilon_2)$  from the discrete spectrum obtained in practice, we had to develop the smoothing procedure (16). The theoretical expressions with exact  $\delta$  functions are also not directly applicable in numerical simulation. One should remember these peculiarities of numerical calculations during the further consideration of previous works.

Our paper resonates with the book of Mott and Davis, where the continuous Kubo-Greenwood formula is presented (see Eq. (2.12) of [50]). Its derivation starts from Fermi's golden rule in the form including DOS (see Eq. (2.8) of [50]).

The book of Messiah contains a rather strict and clear derivation of Fermi's golden rule in the form including DOS (see Eq. (XVII.50) of [57]). It is derived for transitions from a discrete to a continuous spectrum. It is also assumed that matrix elements and density of states are “practically constant over the interval” of final states.

It is not stated explicitly in the book of Mott and Davis whether they consider a continuous spectrum or a discrete one with a small distance between the levels. Some “average over all states having energy near final” is also mentioned. Since the further consideration is mostly theoretical, Mott and Davis do not specify the procedure of averaging or examine whether matrix elements and DOS change smoothly as the functions of final energy. In our numerical calculation, the distance between energy levels is small but finite (Sec. II). Therefore, we cannot omit these questions and have to develop the procedure of smoothing the squares of matrix elements (16).

Theoretical expressions for matrix elements in several cases are also present in [50]. In our paper, we obtain SSME from numerical calculations based on DFT and QMD. In principle, our approach enables the comparison of theoretical models with numerical calculations.

Our paper also resonates with the book of Madelung, which contains the continuous Kubo-Greenwood formula too (see Eq. (8.82) of [51]). For its derivation, the adiabatic switching of the external sinusoidal electric field is considered, and the Liouville–von Neumann equation is solved in the first-order perturbation theory. The discrete spectrum is likely considered; therefore, the usual Kubo-Greenwood formula similar to Eq. (5) is to be obtained. However, the result is immediately written in the form that leads to the continuous Kubo-Greenwood formula (see Eqs. (8.79) and (8.82)

of [51]). Madelung states that “the matrix element is to be averaged over all states in the intervals  $dE$  and  $dE'$ ” but does not specify a formula for this averaging. The more elaborate consideration would be similar to our Secs. III A and III B and include the smoothing procedure (16). The continuous Kubo-Greenwood formula remains mostly a fundamental result in the book of Madelung; little theoretical and no numerical development is present.

The continuous Kubo-Greenwood formula is presented in Eq. (2.34) of [52]. Its derivation reduces to the idea that “if the energy gap between the neighboring states is small, the sum in the exact Kubo-Greenwood formula may be represented as the integral.” However, neither major theoretical development nor numerical implementation of the continuous Kubo-Greenwood formula is further considered in the work [52].

Transport and optical properties of warm dense hydrogen are studied in [53] using QMD and DFT techniques. This paper contains an equation (Eq. (6) of [53]) that may have the meaning of the continuous KG formula (22) or the exact KG formula in the continuous form (34). This equation includes some “analogue of matrix element squared for a continuous range of energies,”  $|D(E', E)|^2$ . The latter expression is not explicitly defined. It may be inferred that some numerical calculation was performed according to Eq. (6) of [53] on the basis of QMD+DFT results. This could be rather close to our approach; however, the details of this calculation, such as the function  $|D(E', E)|^2$ , are not available. The theoretical part of [54] is close to that of [53].

Transport and optical properties of amorphous semiconductors are considered in [55]. Equations (11) and (12) of [55] are close to the exact Kubo-Greenwood formula in the continuous form (34) from our paper. The theoretical expression for matrix elements, containing a free parameter, is obtained within the random phase model. The final value of squared matrix elements multiplied by the square of DOS is deduced from experimental results on transport properties. This allows the author of [55] to blur the difference between the exact Kubo-Greenwood formula in the continuous form and the continuous Kubo-Greenwood formula.

The continuous Kubo-Greenwood formula is presented in Eq. (6.131) of [56]. This formula is discussed only from a theoretical point of view; the numerical implementation is not considered.

In our paper, we apply the continuous Kubo-Greenwood formula to the output of QMD+DFT numerical calculation. Therefore, we need the expression that produces a smooth function  $D(\varepsilon_1, \varepsilon_2)$  from QMD+DFT results. The works [50–56] discussed above do not report such an expression. We use Eq. (16) for that purpose. Several works [58–60] contain expressions close to our Eqs. (16) or (18).

The optical properties of disordered semiconductors are studied using the expression similar to the continuous Kubo-Greenwood formula in the paper of Abe and Toyozawa (see Eq. (1.7) of [58]). The authors aim to analyze the formation of optical properties by studying DOS and squared matrix element  $M(E_1, E_2)$ ; this is close to the motivation of our work. The calculation of squared matrix elements starts from Eq. (3.4) of [58], similar to our Eq. (18). However, the numerator in this expression is calculated using a technique

significantly different from ours: the authors apply the tight-binding (TB) model and perform a numerical calculation on the basis of a theory formulated in terms of the Green's functions. Some model expressions for DOS are also introduced. The work [58] is the only among those considered in this section where the landscape of squared matrix elements  $M(E_1, E_2)$  is plotted.

Some of the ideas and results of [58] are presented more clearly in the work of Cody [59]. He rewrites the exact Kubo-Greenwood formula in the continuous form (see Eqs. (15), (40), and (41) of [59]). Then Cody states that expression (3.4) of [58] for squared matrix elements  $M(E_1, E_2)$  may be reformulated in the form similar to our Eq. (16) (see Eqs. (43) and (44) of [59]). However, the latter equations include exact  $\delta$  functions (in contrast to our paper, in which broadened  $\delta$  functions are used). Other calculations of [58] are not reformulated in this way; only the model and results are then discussed. Consequently, Eqs. (43) and (44) with the exact  $\delta$  functions create no problems for the work [59].

The exact Kubo-Greenwood formula in the continuous form is presented in Eq. (4) of [60]. This paper also contains an expression for matrix elements squared  $M^2(E, E')$  that looks like our Eq. (16) (see Eq. (5) of [60]). However, the exact  $\delta$  functions are used in this expression. Therefore, this expression is not directly applicable for numerical calculations. This does not cause any problems in the paper [60], since they proceed with a theoretical estimation of  $M^2(E, E')$  for amorphous semiconductors.

Though the works [58–60] contain expressions looking like our Eqs. (16) and (18), none of them may be directly used to obtain smooth  $D(\varepsilon_1, \varepsilon_2)$  from QMD+DFT calculations.

Besides ours, other approaches were suggested to analyze the formation of transport and optical properties. Below we discuss some other experimental [61] and computational [62,63] methods.

The optical properties of amorphous and crystalline solids are considered using the Kubo-Greenwood formula in [61]. The exact KG formula (Eq. (3) of [61]) is expressed in a continuous form different from ours. This continuous form (see Eq. (8) of [61]) contains the joint density of states (JDOS)  $J(\hbar\omega)$  and averaged dipole matrix elements squared  $R^2(\hbar\omega)$ . JDOS is connected with the number of transitions corresponding to a given frequency  $\omega$ . The definition of JDOS in [61] is applicable only at rather small electron temperatures. In contrast to our SSME, all matrix elements corresponding to the same frequency  $\omega$  are averaged to form the resulting  $R^2(\hbar\omega)$ . The authors of [61] state that “more general average matrix elements” close to our SSME contain more information from the theoretical point of view. However, only  $R^2(\hbar\omega)$  may be derived from the experiment conducted in [61].

The electronic structure, optical and transport properties of germanene are studied in [62]. For this crystalline two-dimensional material, only two bands, valence and conduction ones, are considered within the tight-binding model. The dependence  $E(\mathbf{k})$  of the electron energy on the wave vector may be traced for each of these bands. The matrix elements of transitions between valence and conduction bands,  $D(\mathbf{k})$ , are then used to calculate optical properties via the usual

Kubo-Greenwood formula. The authors of [62] report not only the final results on optical properties but also the dependence  $|D(\mathbf{k})|^2$ .

In [63], the optical properties of graphene doped with various amounts of silicon are calculated using DFT and the usual Kubo-Greenwood formula. The dependence of electron energy on wave vector  $E(\mathbf{k})$  for various bands may be traced for these crystalline two-dimensional materials. The unfolding procedure [64] is used to switch from the supercell to a smaller cell; this makes the band structure much clearer. The authors investigate the contribution of various initial bands and wave vectors to the integrated dynamic electrical conductivity  $\int \sigma_1(\omega) d\omega$ .

The methods of [62,63] require  $E(\mathbf{k})$ . Therefore they are applicable for crystalline solids with small imperfections.

The performed consideration helps us to estimate the position of our paper among the previous works. In this study, we combine in practice the *continuous* Kubo-Greenwood formula with the numerical calculation based on DFT and QMD methods. We provide the theory necessary for the numerical implementation of the continuous KG formula. In particular, this theory includes the smoothing procedure (16) with the broadened  $\delta$  functions and the proof of the fact that the usual and continuous KG formulas are equivalent in the limit of zero broadening (Sec. IV B). The practical numerical implementation of the continuous Kubo-Greenwood formula in the parallel CUBOGRAM code (Continuous Kubo-Greenwood Program) is the major result of our paper. We demonstrate the capabilities of the CUBOGRAM code by performing calculations for liquid aluminum. Both the values of transport properties and the brief analysis of their formation are reported. Our technique also provides additional opportunities to examine various methods of matrix elements calculation. These methods may be studied deeper by analyzing the function  $D(\varepsilon_1, \varepsilon_2)$  for each case.

## VIII. CONCLUSION

In this work we present the derivation and discussion of the continuous Kubo-Greenwood formula. Our theoretical consideration (Sec. IV B) demonstrates that the continuous formula is a valid alternative to the usual Kubo-Greenwood formula. Both formulas produce close results on dynamic electrical and thermal conductivity. Unlike the usual formula, the continuous one is formulated as the integral of several continuous functions over the electron spectrum: the smoothed squares of matrix elements  $D(\varepsilon, \varepsilon + \hbar\omega)$ , the densities of states  $g(\varepsilon)g(\varepsilon + \hbar\omega)$ , and the difference of the Fermi weights  $f(\varepsilon) - f(\varepsilon + \hbar\omega)$ . We can plot these functions and analyze the contribution of various sections of the electron spectrum to electrical and thermal conductivity (Sec. V). We consider that the possibility of such analysis is the main advantage of the continuous formula.

We also study the dependence of the results on a number of technical parameters. Numerical simulations were performed for liquid aluminum using four different methods of calculating matrix elements. These methods encompass various realizations of “transverse” and “longitudinal” formulas. The parallel CUBOGRAM code has been created to implement

the continuous Kubo-Greenwood formula. Our study demonstrates that the proposed scheme for transport properties calculation is a useful tool for theoretical analysis and qualitative estimations.

#### ACKNOWLEDGMENT

The authors thank the Russian Science Foundation (Grant No. 20-42-04421) for financial support.

- 
- [1] M. Preising and R. Redmer, *Phys. Rev. B* **102**, 224107 (2020).
- [2] S. Kumar, A. J. Poser, M. Schöttler, U. Kleinschmidt, W. Dietrich, J. Wicht, M. French, and R. Redmer, *Phys. Rev. E* **103**, 063203 (2021).
- [3] M. E. Povarnitsyn, P. R. Levashov, and D. V. Knyazev, *Appl. Phys. Lett.* **112**, 051603 (2018).
- [4] G. S. Sarkisov, A. Hamilton, and V. I. Sotnikov, *Phys. Rev. E* **98**, 053203 (2018).
- [5] A. Ravasio, M. Bethkenhagen, J.-A. Hernandez, A. Benuzzi-Mounaix, F. Datchi, M. French, M. Guarguaglini, F. Lefevre, S. Ninet, R. Redmer, and T. Vinci, *Phys. Rev. Lett.* **126**, 025003 (2021).
- [6] G. Faussurier, C. Blancard, and M. Bethkenhagen, *Phys. Rev. E* **104**, 025209 (2021).
- [7] M. Povarnitsyn, N. Andreev, P. Levashov, K. Khishchenko, and O. Rosmej, *Phys. Plasmas* **19**, 023110 (2012).
- [8] K. Eidmann, J. Meyer-ter-Vehn, T. Schlegel, and S. Hüller, *Phys. Rev. E* **62**, 1202 (2000).
- [9] M. E. Povarnitsyn, N. E. Andreev, E. M. Apfelbaum, T. E. Itina, K. V. Khishchenko, O. F. Kostenko, P. R. Levashov, and M. E. Veysman, *Appl. Surf. Sci.* **258**, 9480 (2012).
- [10] Y. T. Lee and R. More, *Phys. Fluids* **27**, 1273 (1984).
- [11] W. Ebeling, A. Förster, V. Fortov, V. Gryaznov, and A. Polishchuk, *Thermophysical Properties of Hot Dense Plasma* (Vieweg+Teubner Verlag, Stuttgart, 1991).
- [12] D. Saumon, G. Chabrier, and H. M. van Horn, *Astrophys. J. Suppl. Ser.* **99**, 713 (1995).
- [13] M. Schlages, M. Bonitz, and A. Tschtschjan, *Contrib. Plasma Phys.* **35**, 109 (1995).
- [14] R. Redmer, *Phys. Rep.* **282**, 35 (1997).
- [15] E. M. Apfelbaum, *Phys. Plasmas* **22**, 092703 (2015).
- [16] T. Dornheim, S. Groth, and M. Bonitz, *Phys. Rep.* **744**, 1 (2018).
- [17] P. Hamann, T. Dornheim, J. Vorberger, Z. A. Moldabekov, and M. Bonitz, *Phys. Rev. B* **102**, 125150 (2020).
- [18] A. Khomkin and A. Shumikhin, *J. Exp. Theor. Phys.* **130**, 602 (2020).
- [19] J. Ziman, *Philos. Mag.* **6**, 1013 (1961).
- [20] E. Apfelbaum, *Phys. Chem. Liq.* **48**, 534 (2010).
- [21] T. Dornheim, A. Cangì, K. Ramakrishna, M. Böhme, S. Tanaka, and J. Vorberger, *Phys. Rev. Lett.* **125**, 235001 (2020).
- [22] E. Runge and E. K. U. Gross, *Phys. Rev. Lett.* **52**, 997 (1984).
- [23] K. Ramakrishna, A. Cangì, T. Dornheim, A. Baczewski, and J. Vorberger, *Phys. Rev. B* **103**, 125118 (2021).
- [24] M. S. Green, *J. Chem. Phys.* **22**, 398 (1954).
- [25] R. Kubo, *J. Phys. Soc. Jpn.* **12**, 570 (1957).
- [26] D. Greenwood, *Proc. Phys. Soc.* **71**, 585 (1958).
- [27] M. P. Desjarlais, J. D. Kress, and L. A. Collins, *Phys. Rev. E* **66**, 025401(R) (2002).
- [28] S. Mazevet, J. Clérouin, V. Recoules, P. M. Anglade, and G. Zerah, *Phys. Rev. Lett.* **95**, 085002 (2005).
- [29] J. Clérouin, P. Noiret, P. Blottiau, V. Recoules, B. Siberchicot, P. Renaudin, C. Blancard, G. Faussurier, B. Holst, and C. Starrett, *Phys. Plasmas* **19**, 082702 (2012).
- [30] Y. V. Petrov, K. P. Migdal, D. V. Knyazev, N. A. Inogamov, and P. R. Levashov, *J. Phys.: Conf. Ser.* **774**, 012103 (2016).
- [31] K. Migdal, V. Zhakhovsky, A. Yanilkin, Y. Petrov, and N. Inogamov, *Appl. Surf. Sci.* **478**, 818 (2019).
- [32] B. Holst, M. French, and R. Redmer, *Phys. Rev. B* **83**, 235120 (2011).
- [33] M. Pozzo, C. Davies, D. Gubbins, and D. Alfe, *Nature (London)* **485**, 355 (2012).
- [34] M. French and T. R. Mattsson, *Phys. Rev. B* **90**, 165113 (2014).
- [35] D. Knyazev and P. Levashov, *Comput. Mater. Sci.* **79**, 817 (2013).
- [36] G. Kresse and J. Hafner, *Phys. Rev. B* **47**, 558 (1993).
- [37] G. Kresse and J. Hafner, *Phys. Rev. B* **49**, 14251 (1994).
- [38] G. Kresse and J. Furthmüller, *Phys. Rev. B* **54**, 11169 (1996).
- [39] D. Knyazev and P. Levashov, *Contrib. Plasma Phys.* **59**, 345 (2019).
- [40] D. V. Knyazev and P. R. Levashov, *Phys. Plasmas* **21**, 073302 (2014).
- [41] L. L. Moseley and T. Lukes, *Am. J. Phys.* **46**, 676 (1978).
- [42] N. W. Ashcroft and N. D. Mermin, *Solid State Physics* (Harcourt, New York, 1976).
- [43] D. V. Knyazev and P. R. Levashov, *Phys. Plasmas* **22**, 053303 (2015).
- [44] G. Kresse and D. Joubert, *Phys. Rev. B* **59**, 1758 (1999).
- [45] J. P. Perdew, K. Burke, and M. Ernzerhof, *Phys. Rev. Lett.* **77**, 3865 (1996).
- [46] M. Gajdoš, K. Hummer, G. Kresse, J. Furthmüller, and F. Bechstedt, *Phys. Rev. B* **73**, 045112 (2006).
- [47] D. Vanderbilt, *Phys. Rev. B* **41**, 7892 (1990).
- [48] J. P. Perdew and A. Zunger, *Phys. Rev. B* **23**, 5048 (1981).
- [49] B. Adolph, J. Furthmüller, and F. Bechstedt, *Phys. Rev. B* **63**, 125108 (2001).
- [50] N. F. Mott and E. A. Davis, *Electronic Processes in Non-Crystalline Materials*, 2nd ed. (Clarendon, Oxford, 1979).
- [51] O. Madelung, *Introduction to Solid-State Theory*, Springer Series in Solid-State Sciences (Springer, Berlin, 1997).
- [52] I. M. Saitov, Ph.D. thesis, Moscow Institute of Physics and Technology, 2013.
- [53] I. Kwon, L. Collins, J. Kress, and N. Troullier, *Phys. Rev. E* **54**, 2844 (1996).
- [54] L. A. Collins, S. R. Bickham, J. D. Kress, S. Mazevet, T. J. Lenosky, N. J. Troullier, and W. Windl, *Phys. Rev. B* **63**, 184110 (2001).
- [55] N. K. Hindley, *J. Non-Cryst. Solids* **5**, 17 (1970).
- [56] G. A. Kobzev, I. T. Iakubov, and M. M. Popovich, *Transport and Optical Properties of Nonideal Plasma* (Springer, Boston, 1995).
- [57] A. Messiah, *Quantum Mechanics: Two Volumes Bound as One* (Dover, New York, 1999).

- [58] S. Abe and Y. Toyozawa, *J. Phys. Soc. Jpn.* **50**, 2185 (1981).
- [59] G. Cody, in *Hydrogenated Amorphous Silicon*, Semiconductors and Semimetals Vol. 21, edited by J. I. Pankove (Elsevier, Amsterdam, 1984), pp. 11–82.
- [60] M. H. Cohen, C. M. Soukoulis, and E. N. Economou, *AIP Conf. Proc.* **120**, 371 (1984).
- [61] W. B. Jackson, S. M. Kelso, C. C. Tsai, J. W. Allen, and S.-J. Oh, *Phys. Rev. B* **31**, 5187 (1985).
- [62] R. Chegel and S. Behzad, *Sci. Rep.* **10**, 704 (2020).
- [63] Y.-T. Lee, C.-C. Lee, M. Fukuda, and T. Ozaki, *Phys. Rev. B* **102**, 075143 (2020).
- [64] W. Ku, T. Berlijn, and C.-C. Lee, *Phys. Rev. Lett.* **104**, 216401 (2010).